

A  
Entered

Duplicate

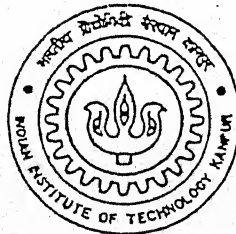
9610526

Dub

# DEVELOPMENT OF THREE-FINGERED PLANAR HAND

by

PANKAJ SHARMA



to the

DEPARTMENT OF MECHANICAL ENGINEERING  
INDIAN INSTITUTE OF TECHNOLOGY, KANPUR

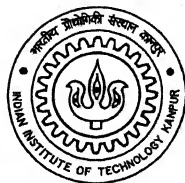
June, 1998

TH  
ME/1998/M  
Sh

# DEVELOPMENT OF THREE-FINGERED PLANAR HAND

*A Thesis Submitted*  
in Partial Fulfilment of the Requirements  
for the Degree of  
Master of Technology

by  
PANKAJ SHARMA



*to the*  
**DEPARTMENT OF MECHANICAL ENGINEERING**  
**INDIAN INSTITUTE OF TECHNOLOGY, KANPUR**

June, 1998

5 FEB 2003 /ME

दृष्टीतः क.जी.नाथ के.के.कर पुस्तकालय  
म.प्र.रा. वि.वि.की संस्थान कामपुर

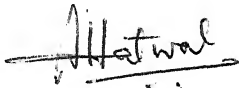
अवधि क्र. A 141996



A141996

## C E R T I F I C A T E

It is certified that the work contained in the thesis entitled **DEVELOPMENT OF THREE-FINGERED PLANAR HAND** by Mr. Pankaj Sharma, has been carried out under my supervision and that this work has not been submitted elsewhere for a degree.



Dr. HIMANSHU HATWAL

Professor

Department of Mechanical Engineering

Indian Institute of Technology, Kanpur

June, 1998



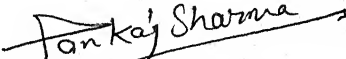
# ACKNOWLEDGMENTS

It is my proud privilege to express my deep sense of gratitude towards my guide Dr. Himanshu Hatwal for giving me valuable guidance and a word of caution whenever I was getting off the rails.

I am obliged to Dr. A. K. Mallik and Dr. A. Mukherjee for the inspiration and the helpful suggestions they have provided. I thank Dr. B. Dasgupta for providing me a friendly company in the lab.

It was a pleasure to be associated with the centre for Robotics for two years and I gained a lot from the discussions. I would like to thank Ms. Anjali Kulkarni, Mr. Susmit Sen and other staff of the lab in this regard. I am also thankful to Mr. Jha, Mr. Sharma and Mr. Namdeo of the manufacturing lab for having helped me in the fabrication of mechanical components.

Finally I appreciate A. Sai kumar, V.Yugandhar and all my other friends for making my stay in IIT a wonderful and a memorable one. I would also like to thank Pulkesh and Anita for painstakingly assisting in completion of the thesis.

  
Pankaj Sharma.

# Abstract

The need of the multifingered mechanical hands as dexterous end-effectors for robotic devices has been widely felt due to their capability and versatility. In the present work basic theory for multifingered hands is presented. The position and orientation of the fingertips and the object with reference to the base of the hand is calculated as a function of joint variables using forward kinematics. Controller scheme is presented for tracking a specified trajectory of a grasped object. Dynamic equations of motion are used to develop a mathematical model for the controller. Grasping force control issue is also considered covering the issues of the contact point stability criterion and grasp stability. Concept of coefficient of friction angle is also introduced to compare actual grasp with ideal stable grasp. Finger links and base plate are designed. The criteria for selection of motor/power drive is also discussed. Strain gauges are used to measure the transverse force applied at the fingertip. Scheme for the required electronic circuitry is also presented. Object grasp is accomplished under static conditions.

# Contents

<b>Acknowledgments</b>	<b>i</b>
<b>Abstract</b>	<b>ii</b>
<b>List of Figures</b>	<b>v</b>
<b>List of Tables</b>	<b>vii</b>
<b>1 Introduction</b>	<b>1</b>
1.1 Introduction	1
1.2 Literature Review	2
1.3 Objective and Scope of the Present Work	3
<b>2 Multifingered Planar Hand Kinematics</b>	<b>4</b>
2.1 Introduction	4
2.2 Forward Kinematics	5
2.2.1 Basic Relations	5
2.2.2 Constraints	5
2.2.3 Finger Kinematics	7
2.2.4 Finger-Object System Kinematics	10
2.2.5 Grip Transformation Matrix	15
2.3 Static Force Equations	17
2.3.1 Static Force at Contact Points	17
2.3.2 Static Force at Origin of Object Frame	18

<b>3</b>	<b>Control Scheme</b>	<b>19</b>
3.1	Introduction	19
3.2	Equations of Motion	20
3.3	Controller Model	22
	3.3.1 State Feedback Controller	26
3.4	Control of Grasping Force	28
	3.4.1 Optimal Grasping Strategy	29
	3.4.2 Grasping Force Considerations	31
<b>4</b>	<b>Design Details</b>	<b>33</b>
4.1	Introduction	33
4.2	Finger Design	34
4.3	Motor Selection and Specifications	42
4.4	Force Sensing using Strain Gauges	45
<b>5</b>	<b>Implementation, Results and Discussions</b>	<b>50</b>
5.1	Strain Gauge Calibration	50
5.2	Amplification of Bridge Output	52
5.3	The Controller Board	54
5.4	Feedback Board	60
5.5	Results and Discussions	61
	<b>Bibliography</b>	<b>68</b>

# List of Figures

2.1	Planar non-redundant 3-fingered hand grasp constraints	6
2.2	Planar hand and object schematic	7
2.3	$i^{\text{th}}$ Finger schematic in World Coordinate Frame	8
2.4	Finger arrangement schematic	8
2.5	Object frames schematic	11
2.6	Velocity of the $i^{\text{th}}$ contact point	15
2.7	$i^{\text{th}}$ contact point schematic	16
3.1	Representation of a translated object frame	21
3.2	Defining the grasping force parameter $\lambda_h$	23
3.3	Block diagram for the closed-loop control	27
3.4	Schematic representation for a typical contact case	29
4.1	Planar hand joint axes schematic	34
4.2	Object position and orientation schematic	35
4.3	Finger links arrangement schematic	36
4.4	Link assembly schematic	36
4.5	Provision for clamping of shaft	37
4.6	Strain gauge mounting schematic	37
4.7	Link-1 dimensions	38
4.8	Link-2 dimensions	38
4.9	Fingertip covering schematic	39
4.10	Overall finger arrangement	39
4.11	Base plate dimensions	40
4.12	Object dimensions	40
4.13	Top view of the actual setup	41
4.14	Motor operating range	44

4.15	Dimensions for the selected motor	45
4.16	Resolving the components of the contact force $F_c$	46
4.17	Wheatstone bridge arrangement for measurement of $(F_c)_t$	46
4.18	Wheatstone bridge arrangement for measurement of $(F_c)_n$	47
4.19	PCB diagram for measurement of $(F_c)_t$	48
4.20	Force feedback schematic	49
5.1	Graphical representation of calibration results	52
5.2	Output voltage amplification schematic	52
5.3	Pulse width modulation with square wave form	55
5.4	Schematic for combined pulse width modulation	55
5.5	Block diagram for L-298 dual full bridge driver	56
5.6	PCB diagram for the controller board	58
5.7	PCB diagram for the feedback board	59
5.8	Nomenclature convention for motors and fingers	60

# List of Tables

4.1	Basic features of the motor used	42
4.2	Important motor specifications	43-44
4.3	Strain gauge specifications	49
5.1	Calibration chart for strain gauges	51
5.2	Signals for different motor motions	57
5.3	Output voltage observations	61
5.4	Conversion chart	62
5.5	rms. Voltage observations	62
5.6	Current and torque calculations	63
5.7	Measured joint angles	63
5.8	Transverse components for the three-fingers	66

# **Chapter 1**

## **Introduction**

---

### **1.1 Introduction**

The need of multifingered mechanical hands as dexterous end-effectors for robotic devices has been widely felt. Such capabilities of these devices range from securely grasping a broad range of objects to performing fine manipulation tasks. Apart from dexterity, multifingered hands are also versatile devices which can serve various purposes ranging from a simple manipulation to complicated assembly operations. Grasping of an object by a computer-controlled hand is an important task because it precedes any other movement of the object by the hand. Also it is the point at which uncertainty in the position and orientation of an object is first encountered. The purpose of this work is to develop an understanding of the theory of manipulation and using it for the development of a three-fingered planer hand.



## 1.2 Literature Review

Probably the first occurrence of mechanical hands was in prosthetic devices to replace lost limbs. Almost without exception prosthetic hands have been designed to simply grip objects. Other related field in which artificial hands have found use is in remote manipulation. The need to work with hazardous materials or environments has spawned the development of master-slave or teleoperated systems. These devices permit the user to perform simple manipulations from a safe remote location by employing mechanical arms directly controlled by the operator through electrical or mechanical means.

Significant hand design attempts were made by Okada[Okada, 1979] and Salisbury[Salisbury, 1989]. Cutkosky[Cutkosky, 1985] developed a procedure for analyzing the grasp properties of stiffness and resistance to slipping, in order to compare grasps. Kerr and Roth[Kerr, 1986] formulated the linearized constraint concerning the fingertip forces due to the fingertip contact and proposed an optimal selection of the fingertip force in a static grasp using linear programming. The problem of stable grasp in a plane is discussed in [Nguyen, 1986]. Kobayashi[Kobayashi, 1986] discussed the control and geometric aspects for an articulated robot hand. Fearing[Fearing, 1986] and Omata[Omata, 1994] discussed a new force strategy for object reorientation. Kumar and Waldron[Kumar, 1989] proposed a sub-optimal method for grasping force computation, based on the superposition of finger-interaction forces on force equilibrium. Cole, Hsu and Sastry[Cole, 1992] considered the problem of dynamic control of a multifingered hand manipulating an object under the condition that some of the fingertips slide on the object surfaces. Schemes and algorithms for finding the optimal fingertip forces were offered by Nahon and Angeles[Nahon, 1992], Mukerjee and Waldron[Mukerjee, 1992], Guo and Gruver[Guo, 1993] and Shimoga[Shimoga, 1996]. The control strategies were offered by Chung and Waldron[Chung, 1995]. Kvrđic[Kvrđic, 1996] proposed a new method for computing the grasping forces of the object grasped by multiple cooperating manipulators or a multifingered robot hand. The iterative algorithm for predicting grasping force and moment components, satisfying their limitations and condition of the minimal internal loading, was proposed. Mackawa, Tanic and

Komoriya[Mackawa, 1996] proposed dynamic grasping force control for a multifingered hand and experimentally confirmed the validity of the proposed method using a two-fingered hand with finger-shaped tactile sensors.

## 1.3 Objective and Scope of the Present Work

This work attempts to solve the problem of development of a three-fingered planar hand. Initially positions of the fingertips and the object in the base frame is found out. Using static force equations, contact force and the force at the origin of the object frame is found. The controller is modeled and the mechanical parts are designed. Strain gauges are used for the force feedback for the transverse force. Scope of present work is to provide real-time closed-loop trajectory control.

This thesis has been organized into five chapters. In chapter 2 the problem of multifingered hand kinematics is introduced. Forward kinematics solution for the finger-object system is presented. Equations for computing static force at fingertip-object contact points and at the origin of the object frame are presented. In chapter 3 dynamic equations of motion are discussed in brief. A controller model is presented and grasping force is discussed. In chapter 4 design details are given. Various parts of the finger are discussed. Motor selection criterion is also given. Force sensing scheme for strain gages is also presented. In chapter 5 the strain gauge calibration data is given. Amplification scheme for the Wheatstone bridge output is discussed. The controller board and feedback board are discussed. Finally the results and discussions are presented.

## **Chapter 2**

# **Multifingered Planer Hand Kinematics**

---

## **2.1 Introduction**

Finger kinematics deals with the study of the mapping of joint coordinates to fingertip coordinates in motion, and the inverse mapping of fingertip coordinates to joint coordinates in motion. To study the geometrical and time based properties of the manipulator motion, analysis of the hand kinematics is presented. In this chapter, position and orientation of the finger links in static situations are considered. In order to deal with the geometry of a finger, frames are attached to various parts of the links and then the relationship between these frames is described. Hand kinematics also involves the change of location of these frames as the links articulate. The central topic of the present chapter is basic theory and method to compute the position and orientation of the fingertips and the object relative to the base of the hand as a function of joint variables.

## 2.2 Forward Kinematics

For manipulation of an object in a required manner, knowledge of object position and orientation is essential at all instants of time. If the fingers do not leave contact with the object and if the fingers do not slip over the object surface, the position and orientation of the object can be determined with the help of forward kinematics relations from the measurement of joint angles of the finger joints. Forward kinematics is the static geometrical problem of computing the position and orientation of fingertips and object relative to the base frame.

### 2.2.1 Basic Relations

Let us consider a multifingered planer hand consisting of  $N_f$  fingers, each finger having  $N_d$  degrees of freedom. Task space dimension  $N_t = 2$  and the object degree of freedom  $N_p = 3$ .

To define position and orientation of a body in a plane, specifications of coordinates of two points on a body are required; thus at least two fingers are necessary to grasp an object in a planer hand [Montana, 1995]. Hence for a planer hand case  $N_f \geq 2$ . It is sufficient to have non-redundant fingers [ $N_d = N_t$ ], because each finger only positions the contact point on the object at a particular point of space in the task space. Therefore, in the planer hand, number of links in each finger is taken as two.

### 2.2.2 Constraints

In order to maintain contact with the object surface, fingers have to follow some constraints. The total number of constraints  $N_c$ , to be satisfied by non-redundant fingers [ $N_d = N_t = 2$ ] in order to maintain the contact with the object having degrees of freedom  $N_p = 3$ , are such that  $N_c = (N_f N_d - N_p) = (2N_f - 3)$ .

For the present analysis Coulomb Friction Model is considered for the contact between the object and fingertips. As in [Mason, 1986], the fingers are assumed to grasp the object at their tips. This ensures a point contact and a

fingertip grasp which is essential for dexterous manipulation as discussed in [Cutkosky, 1989]. The object is assumed to be a rigid body. As the object is rigid, the distance between any two finger contact points is constant and it serves as a constraint for proper contact as shown in Fig.(2.1) for  $N_f = 3$ .  $C^i$  is the contact point for the  $i^{th}$  fingertip, where  $i = 1, 2, 3$ .

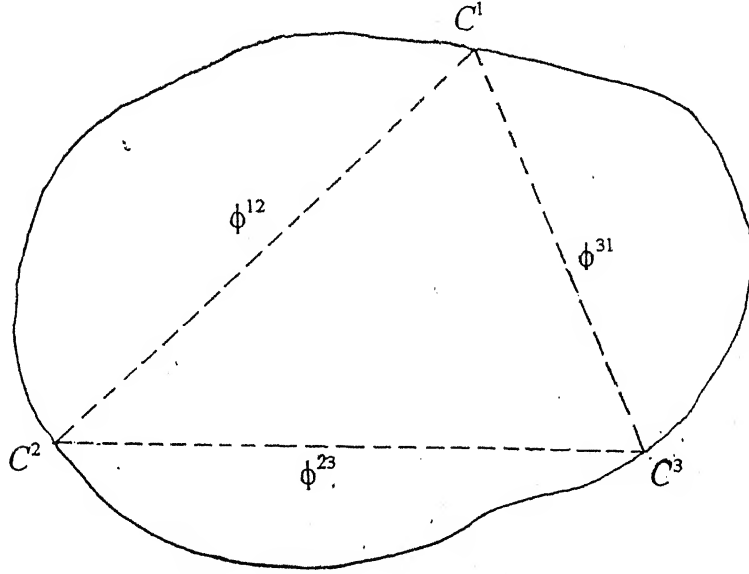


**Figure 2.1 : Planer Non-redundant 3-Fingered Hand Grasp Constraints**

The constraints can be represented as

$$\phi^{i(i+1)} = (\|x^i - x^{(i+1)}\| - d^{i(i+1)}) = 0 \quad (2.1)$$

where  $\phi^{i(i+1)}$  is the constraint between the  $i^{th}$  and  $(i+1)^{th}$  finger,  $x^i$  and  $x^{(i+1)}$  are the position vectors of the corresponding fingertips in the World Coordinate Frame and  $d^{i(i+1)}$  is the distance between the corresponding contact points.

Since  $x^i$  and  $x^{(i+1)}$  are functions of joint variable vector  $\theta$  from forward kinematics,  $\phi^{i(i+1)}$  is also a function of  $\theta$ . Thus the constraints can be combined and written as

$$\phi(\theta) = 0 \quad (2.2)$$

### 2.2.3 Finger Kinematics

For the  $i^{th}$  finger of a multifingered mechanical hand having  $N_f$  fingers in order to represent the position vector  $X^i$  of the fingertip in the World Coordinate Frame  $O_w X_w Y_w Z_w$ , the forward kinematics relations are defined as a function of joint variables  $\theta^i$

$$X^i = f(\theta^i) \quad (2.3)$$

where  $X^i$  is the fingertip position vector of the order  $N_f \times 1$  and  $\theta^i$  is the finger joint variable vector of the order  $N_d \times 1$ .

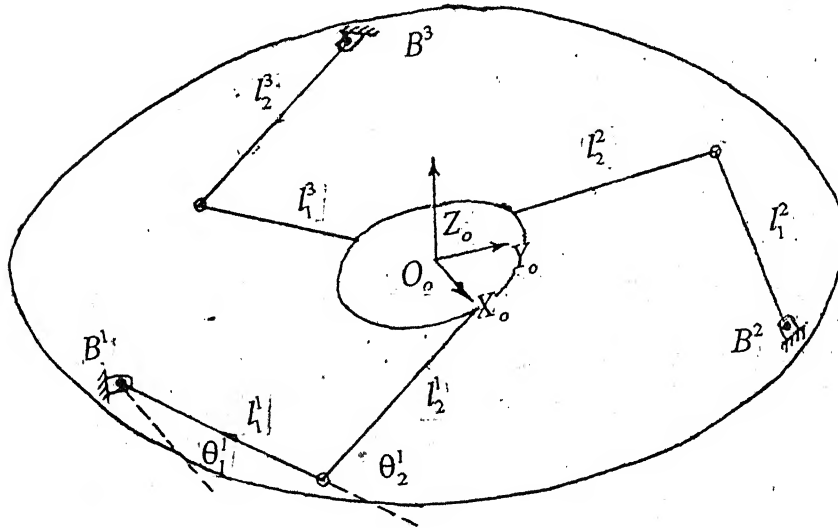
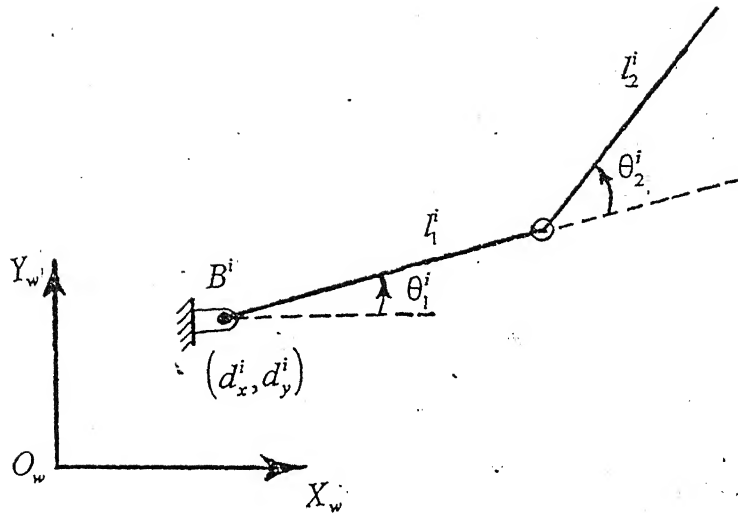


Figure 2.2 : Planer Hand and Object Schematic

For the selected planer hand with  $N_f = 3$ ,  $N_d = 2$ , the fingertip coordinates for the  $i^{th}$  finger ( $i = 1, 2, 3$ ) can be defined as

$$\begin{aligned} x^i &= l_1^i \cos \theta_1^i + l_2^i \cos(\theta_1^i + \theta_2^i) + d_x^i \\ y^i &= l_1^i \sin \theta_1^i + l_2^i \sin(\theta_1^i + \theta_2^i) + d_y^i \end{aligned} \quad (2.4)$$

where  $l_1^i, l_2^i$  is the length of respectively the first and second link for the  $i^{th}$  finger,  $\theta_1^i, \theta_2^i$  is joint angle for the  $i^{th}$  finger and  $(d_x^i, d_y^i)$  is the coordinate of the  $i^{th}$  finger base  $B^i$  in the World Coordinate Frame as shown in Figs.(2.2) and (2.3).



**Figure 2.3 :  $i^{\text{th}}$  Finger Schematic in World Coordinate Frame**

Thus position vector of the fingertip of  $i^{\text{th}}$  arm is written as

$$X^i = \begin{bmatrix} x^i \\ y^i \end{bmatrix} \quad (2.5)$$

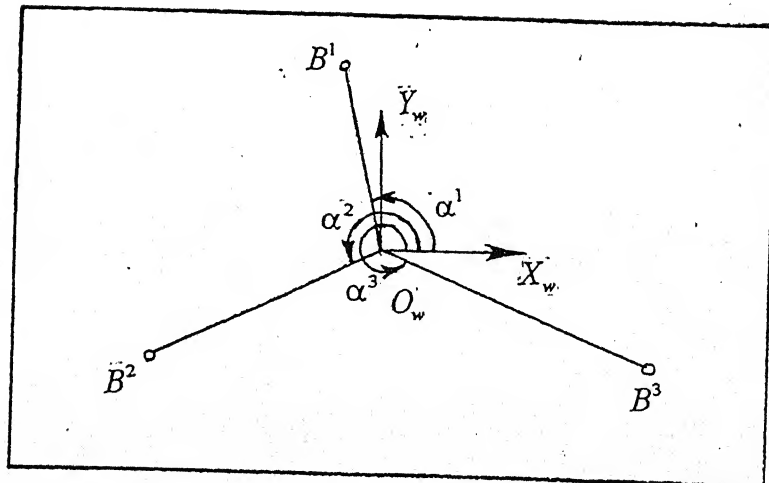


**Figure 2.4 : Finger Arrangement Schematic**

Fig.(2.4) shows the arrangement of the base  $B^i$  of the  $i^{\text{th}}$  finger on the base plate for  $N_f = 3$ .  $\alpha^i$  is the angle measured from positive x-axis in the World Coordinate Frame at which the  $i^{\text{th}}$  base point  $B^i$  is situated.

Velocity vector :

The velocity relation for the  $i^{th}$  finger, which relates the joint velocity and the fingertip velocity can be obtained by differentiating equation(2.3) with respect to time

$$\dot{X}^i = v_c^i = \frac{\partial f}{\partial \theta^i} \dot{\theta}^i \quad (2.6)$$

or, 
$$v_c^i = J_f^i \dot{\theta}^i \quad (2.7)$$

where  $v_c^i$  is the fingertip velocity vector,  $J_f^i = \frac{\partial f}{\partial \theta^i}$  is the Jacobian Matrix of the  $i^{th}$  finger and  $\dot{\theta}^i$  is the joint velocity vector. The orders of  $v_c^i$ ,  $J_f^i$  and  $\dot{\theta}^i$  for the selected planer hand are  $2 \times 1$ ,  $2 \times 2$  and  $2 \times 1$  respectively.

Finger Jacobian :

The Jacobian is a multidimensional form of the derivative. Thus for the  $i^{th}$  finger the Jacobian can be represented as [Duffy, 1996]

$$J_f^i = \frac{\partial f}{\partial \theta^i} \quad (2.8)$$

where  $\partial f$  is the function of joint angles and it represents position of the tip of the finger.

For a planer hand, as shown in [Craig, 1986] the Jacobian for  $i^{th}$  finger can be written as

$$J_f^i = \begin{bmatrix} -L_1^i \sin \theta_1^i - L_2^i \sin(\theta_1^i + \theta_2^i) & -L_2^i \sin(\theta_1^i + \theta_2^i) \\ L_1^i \cos \theta_1^i + L_2^i \cos(\theta_1^i + \theta_2^i) & L_2^i \cos(\theta_1^i + \theta_2^i) \end{bmatrix} \quad (2.9)$$

The combined Finger Jacobian Matrix can be written as

$$J_f = \text{Diag}(J_f^1 \quad J_f^2 \quad \dots \quad J_f^{N_f}) \quad (2.10)$$

where  $N_f$  is the number of fingers.



For planer hand  $J_f$  is a  $6 \times 6$  matrix as discussed in [Fu, 1987].

Rate kinematics :

Using the velocity vector of the fingertip for the  $i^{th}$  finger [equation(2.6)], the combined fingertip velocity vector can be written as

$$v_c = J_f \dot{\theta} \quad (2.11)$$

where  $v_c = [(v_c^1)^T \quad (v_c^2)^T \quad \dots \quad (v_c^{N_f})^T]^T$  is the combined fingertip velocity vector and  $J_f = \text{Diag}(J_f^1 \quad J_f^2 \quad \dots \quad J_f^{N_f})$ .

## 2.2.4 Finger-Object System Kinematics

For an object, the origin  $O_o$  of the object coordinate system is arbitrarily selected at any point in the object and the frame  $O_o X_o Y_o Z_o$  is fixed to the object. In order to relate the position and orientation of the Object Frame  $O_o X_o Y_o Z_o$  with reference to World Frame  $O_w X_w Y_w Z_w$ , a new object frame is taken and a transformation matrix is defined for transformation from object coordinate system to world coordinate system.

Three non-collinear contact points are assumed on the object surface (Fig. 2.5), which can be represented in World Coordinate Frame as a function of joint angles as shown in equation(2.3).

$X^1, X^2$  and  $X^3$  are  $N_t \times 1$  position vectors in World Coordinate Frame for contact points  $O_1, O_2$  and  $O_3$  respectively for the selected planer hand with  $N_f = 3$ ;  $N_t = 2$  is the dimension of the task-space and  $\theta_1, \theta_2, \theta_3$  represent  $N_d \times 1$  finger joint variable vectors,  $N_d = 2$  being the degree of freedom for each finger. It is to be noted that three non-collinear contact points are sufficient to define the new coordinate frame.

Let us define two vectors  $O_{12}$  and  $O_{32}$  such that

$$O_{12} = \frac{(X^1 - X^2)}{\|X^1 - X^2\|}, \text{ and} \quad (2.12)$$

$$O_{32} = \frac{(X^3 - X^2)}{\|X^3 - X^2\|} \quad (2.13)$$

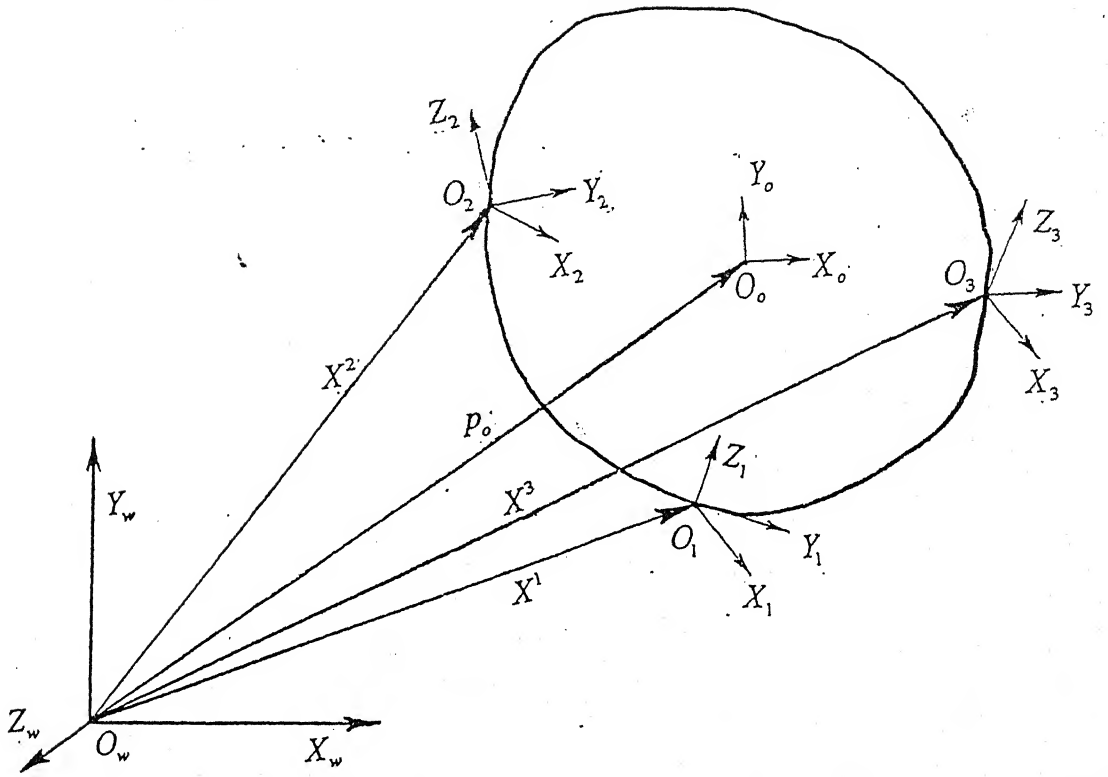


**Figure 2.5 : Object Frames Schematic**

As shown in Fig.(2.5), let us take a new object frame  $O_2X_2Y_2Z_2$ , with origin at  $O_2$ , which could be expressed with the help of unit vectors  $\bar{o}_2\bar{x}_2$ ,  $\bar{o}_2\bar{y}_2$ ,  $\bar{o}_2\bar{z}_2$  along  $O_2X_2$ ,  $O_2Y_2$ ,  $O_2Z_2$  respectively.

$$\bar{o}_2\bar{x}_2 = O_{12} = \frac{(X^1 - X^2)}{\|X^1 - X^2\|} \quad [\text{unit vector along } o_2x_2] \quad (2.14)$$

$$\bar{o}_2\bar{y}_2 = (O_{12} \times O_{32}) \times O_{12} \quad [\text{unit vector along } o_2y_2] \quad (2.15)$$

$$\bar{o}_2\bar{z}_2 = O_{12} \times O_{32} \quad [\text{unit vector along } o_2z_2] \quad (2.16)$$

Thus for the planer hand

$$\bar{o}_2 \bar{x}_2 = \frac{(x^1 - x^2)\hat{i} + (y^1 - y^2)\hat{j}}{[(x^1 - x^2)^2 + (y^1 - y^2)^2]^{\frac{1}{2}}} \quad (2.17)$$

$$\bar{o}_2 \bar{y}_2 =$$

$$\frac{[\{(x^3 - x^2)(y^1 - y^2)^2 - (x^1 - x^2)(y^1 - y^2)(y^3 - y^2)\}\hat{i} + \{(x^1 - x^2)^2(y^3 - y^2) - (x^1 - x^2)(x^3 - x^2)(y^1 - y^2)\}\hat{j}]}{[(x^1 - x^2)^2 + (y^1 - y^2)^2][(x^3 - x^2)^2 + (y^3 - y^2)^2]^{\frac{1}{2}}} \quad (2.18)$$

The homogeneous transformation matrix  ${}^wT_2$ , for representation of Object Frame  $O_2X_2Y_2Z_2$  in the World Coordinate Frame, can be expressed as

$${}^wT_2 = \begin{bmatrix} \bar{o}_2 \bar{x}_2 & \bar{o}_2 \bar{y}_2 & X^2 \\ 0 & 0 & 1 \end{bmatrix} \quad (2.19)$$

since for the planer case, z-components are taken out.

Let a matrix  ${}^2T_o$  is defined, which represents the Object Frame  $O_oX_oY_oZ_o$  in the new frame  $O_2X_2Y_2Z_2$ . Matrix  ${}^2T_o$  is a constant matrix, since the object is assumed to be rigid and both frames  $O_2X_2Y_2Z_2$  and  $O_oX_oY_oZ_o$  are fixed to the object. Thus the matrix  ${}^2T_o$  is a transformation matrix representing frame  $O_oX_oY_oZ_o$  in frame  $O_2X_2Y_2Z_2$ .

Thus the transformation matrix  ${}^wT_o$  representing Object Frame  $O_oX_oY_oZ_o$  in the World Frame  $O_wX_wY_wZ_w$  can be written as

$${}^wT_o = {}^wT_2 {}^2T_o \quad (2.20)$$

The constant transformation matrix  ${}^2T_o$  can be computed once and for all at the time of grasping assuming that at the time of grasping, the representation of object frame in World Coordinate Frame  ${}^wT_o$  is known, i.e., the rotation matrix  ${}^wR_o$  representing the orientation of object frame in World Coordinate Frame and the position vector  $p_o$  denoting the position of the origin of the object frame with respect to the world frame is known at the time of initial grasping.

Thus at the time of initial grasping

$${}^wT_o = \begin{bmatrix} {}^wR_o & p_o \\ O^T & 1 \end{bmatrix} \quad (2.21)$$

The transformation matrix  ${}^wT_o$  is parametrized by three independent parameters; one for orientation in World Coordinate Frame about z-axis and two for position of the object frame origin in World Coordinate Frame. These parameters physically represent the position and orientation of the object in the World Coordinate Frame.

Thus

$${}^wR_o = R_z = \begin{bmatrix} \cos \psi_z & -\sin \psi_z & 0 \\ \sin \psi_z & \cos \psi_z & 0 \\ 0 & 0 & 1 \end{bmatrix} \quad (2.22)$$

where  $\psi_z$  is the angle of rotation of object frame  $O_oX_oY_oZ_o$  about the axis  $O_wZ_w$  of the World Coordinate Frame  $O_wX_wY_wZ_w$  and  $R_z$  is the rotation matrix for rotation about z axis.

Thus the position and orientation, as discussed in [Nof, 1985] for the general case, of the Object Frame in the World Frame, can be represented vectorially as

$$y = \begin{bmatrix} p_o^T \\ \psi_o^T \end{bmatrix} \quad (2.23)$$

where  $y$  is  $6 \times 1$  vector representing the position and orientation of the object,  $p_o = [p_{o_x} \ p_{o_y} \ p_{o_z}]^T$  is the position vector of object frame origin in World Coordinate Frame and  $\psi_o = [\psi_x \ \psi_y \ \psi_z]^T$  is orientation vector containing roll-pitch-yaw coordinates.

For the planar hand, the equation(2.23) reduces to

$$y = \begin{bmatrix} p_{o_x} \\ p_{o_y} \\ \psi_z \end{bmatrix}, \quad (2.24)$$

where  $p_{o_x}, p_{o_y}$  denote position vector components in x and y direction and  $\psi_z$  represents orientation of the object about z-axis in World Coordinate Frame .

As the position and orientation of object in World Coordinate Frame can be denoted as a function of joint angles  $\theta$ , the generalized position vector  $y$  can be represented as

$$y = h_o(\theta) \quad (2.25)$$

where  $h_o(\theta)$  is a function of joint angles, such that  $h_o(\theta) = \begin{bmatrix} p_o^T \\ \psi_o^T \end{bmatrix}$ .

Rate kinematics :

For the finger-object system rate kinematics equations can be obtained by differentiating equation (2.25) with respect to time as

$$\dot{y} = \frac{\partial h_o}{\partial \theta} \dot{\theta} \quad (2.26)$$

$$\text{or,} \quad \dot{y} = J_h \dot{\theta} \quad (2.27)$$

where  $\dot{y}$  is combined linear and angular velocity vector of the object in World Coordinate Frame,  $\dot{\theta}$  is combined finger joint velocity vector and  $J_h$  is hand Jacobian matrix.

Hand Jacobian  $J_h$  for a planar hand is a matrix of order  $3 \times 6$ , which can be written as

$$J_h = \begin{bmatrix} \frac{\partial p_{o_x}}{\partial \theta} \\ \frac{\partial p_{o_y}}{\partial \theta} \\ \frac{\partial \psi_z}{\partial \theta} \end{bmatrix} \quad (2.28)$$

where  $p_{o_x}, p_{o_y}$  denote position and  $\psi_z$  represents orientation of the object in World Coordinate Frame for a planer hand case.

### 2.2.5 Grip Transformation Matrix

Grip Transformation Matrix is the relationship of object and joint velocity vectors as discussed in [Yoshikawa, 1990]. Let for an object  $c^i = (c_x^i \ c_y^i \ c_z^i)^T$  is the position vector of the  $i^{th}$  contact point in the object frame.

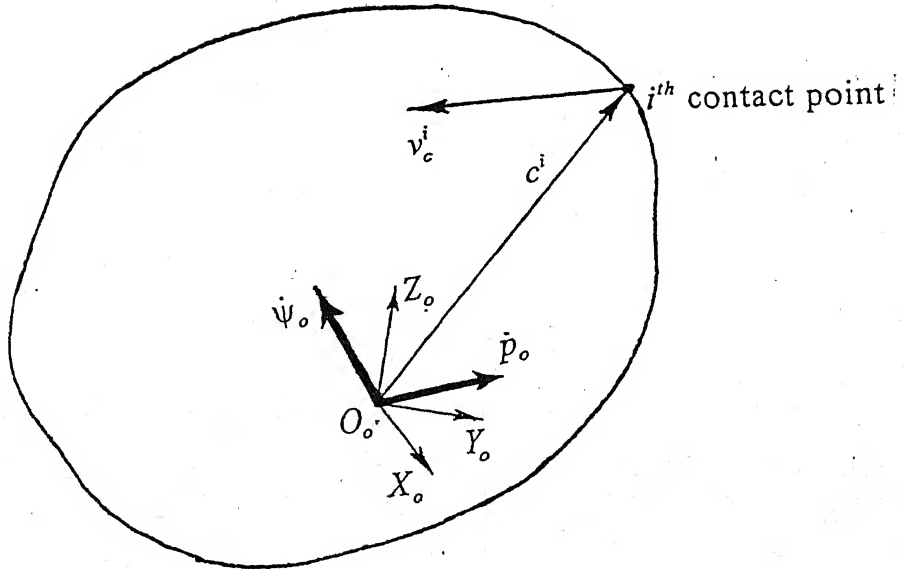


Figure 2.6 : Velocity of the  $i^{th}$  contact point

Given the linear and angular velocity vectors  $\dot{p}_o$  and  $\dot{\psi}_o$  respectively, of the object frame; the velocity of the  $i^{th}$  contact point as shown in Fig.(2.6) can be written as

$$v_c^i = \dot{p}_o + \dot{\psi}_o \times c^i \quad (2.29)$$

or, 
$$v_c^i = G^i \dot{y} \quad (2.30)$$

where  $v_c^i$  represents the velocity vector of  $i^{th}$  contact point,

$\dot{y} = (p_o^T \ \psi_o^T)^T$ , and

$$G^i = \begin{bmatrix} 1 & 0 & -c_y^i \\ 0 & 1 & c_x^i \end{bmatrix} \quad (2.31)$$

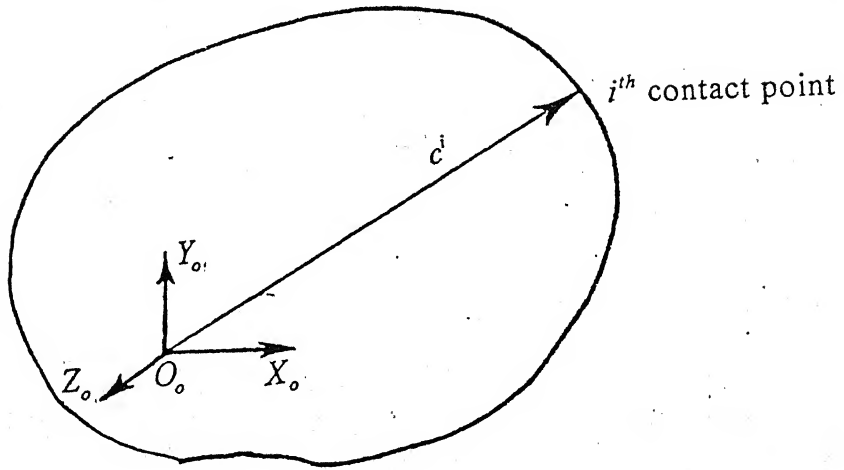


**Figure 2.7 :  $i^{th}$  contact point schematic**

The schematic diagram for representation of  $i^{th}$  contact point in Object Frame is shown in Fig.(2.7).

Combined velocity vector  $V_c$  for all contact points can be written as

$$v_c = G \dot{y} \quad (2.32)$$

where  $v_c = [(v_c^1)^T \ (v_c^2)^T \ \dots \ (v_c^{N_f})^T]^T$ ,  $N_f$  is the number of fingers,  $G = [G^1 \ G^2 \ \dots \ G^{N_f}]^T$  Grip Transform Matrix and  $\dot{y}$  is  $[\dot{p}_o^T \ \dot{\psi}_o^T]^T$ .

Combining equations(2.11) and (2.32) as discussed in [Cole, 1992]

$$G \dot{y} = J_f \dot{\theta} \quad (2.33)$$

The Moore-Penrose Inverse [Rao, 1971] of the Grip Transform Matrix  $G$  is defined as

$$G^{\#T} = G(G^T G)^{-1} \quad (2.34)$$

## 2.3 Static Force Equations

We consider a situation in which all the joints of a manipulator are locked so that it becomes a structure. Then each link in this structure is considered and force-moment balance relationship is written in terms of link frames. Finally, solution for the set of joint torques needed to support a static load acting at the finger tip and to keep the system in static equilibrium is calculated.

### 2.3.1 Static Force At Contact Points

The torque vector ( $\tau$ ) [torque at the link joints], the finger Jacobian matrix ( $J_f$ ), and Cartesian force-moment vector ( $F_c$ ) acting at the fingertips are related as [Klafter, 1989]

$$\tau = J_f^T F_c \quad (2.35)$$

For the planer hand case,

$$\tau = \begin{bmatrix} \tau_1^T \\ \tau_2^T \\ \tau_3^T \end{bmatrix}_{6 \times 1} \quad (2.36)$$

where  $\tau^i$  ( $i=1,2,3$ ) is the torque at the joints of the  $i^{th}$  finger such that  $\tau^i = [\tau_1^i \ \tau_2^i]^T$ ,  $J_f = \text{Diag}(J_f^1 \quad J_f^2 \quad J_f^3)$  is the combined finger Jacobian [as given in equations(2.9) and (2.10)],  $F_c = \begin{bmatrix} F_c^{1T} & F_c^{2T} & F_c^{3T} \end{bmatrix}^T$  is the combined force vector for all contact points such that  $F_c^i = \begin{bmatrix} F_{c_x}^i & F_{c_y}^i \end{bmatrix}$ .



### 2.3.2 Static Force at Origin of Object Frame

The Generalized Force Vector  $F_o$  acting at the origin of the Object Frame  $O_oX_oY_oZ_o$ , is defined in terms of combined force vector  $F_c$  at the contact points as [Mason, 1986]

$$F_o = G^T F_c = \begin{bmatrix} 1 & 0 & 1 & 0 & 1 & 0 \\ 0 & 1 & 0 & 1 & 0 & 1 \\ -c_y^1 & c_x^1 & -c_y^2 & c_x^2 & -c_y^3 & c_x^3 \end{bmatrix} \begin{bmatrix} F_{c_x}^1 \\ F_{c_y}^1 \\ F_{c_x}^2 \\ F_{c_y}^2 \\ F_{c_x}^3 \\ F_{c_y}^3 \end{bmatrix} \quad (2.37)$$

where  $G_{6 \times 3}$  is the grip transformation matrix as defined in equation(2.32),  $c^i = (c_x^i \ c_y^i)^T$  is the position vector for the  $i^{th}$  contact point ( $i = 1, 2, 3$ ) in the object frame and  $F_c^i$  is the contact force at the  $i^{th}$  contact point as defined in equation(2.35).

Also,

$$F_o = \begin{bmatrix} F_{o_x} \\ F_{o_y} \\ M_{o_z} \end{bmatrix} = \begin{bmatrix} F_{c_x}^1 + F_{c_x}^2 + F_{c_x}^3 \\ F_{c_y}^1 + F_{c_y}^2 + F_{c_y}^3 \\ -c_y^1 F_{c_x}^1 + c_x^1 F_{c_y}^1 - c_y^2 F_{c_x}^2 + c_x^2 F_{c_y}^2 - c_y^3 F_{c_x}^3 + c_x^3 F_{c_y}^3 \end{bmatrix} \quad (2.38)$$

where  $F_{o_x}, F_{o_y}$  are the x and y components of the forces at the origin  $O_o$  of the Object Frame  $O_oX_oY_oZ_o$  and  $M_{o_z}$  is the moment about z-axis at  $O_o$ .

We can also write as

$$\tau = J_h^T F_o = J_h^T G^T F_c \quad (2.39)$$

where  $J_h$  is the hand Jacobian matrix [as defined in equations(2.26)-(2.28)].

# Chapter 3

## Control Scheme

---

### 3.1 Introduction

Control is the process of making a variable or system of variables confirm to what is desired. In this chapter, control scheme for tracking a specified trajectory of a grasped object is discussed. Here, all the equations have been developed for a three-fingered planer hand, each finger having two degress-of-freedom. Initially mathematical model for the controller is presented. Equations of motion are used to develop the model but physically no dynamics are involved. Position, orientation, system constraints and grasping force parameters, which are taken as input, are converted to new input vector  $\pi = [\pi_1^T \ \pi_2^T \ \pi_3^T]^T$  using controller equations and overall controller is modeled. Also control of grasping force is discussed covering the issues of contact point stability criterion and grasp stability. Concept of coefficient of friction angle (c.f.a.) is introduced to compare actual grasp with ideal stable grasp.

## 3.2 Equations of motion

The dynamic equation for the complete hand can be derived by combining the dynamics of the fingers with the dynamics of object through the contact constraints [Cole, 1992].

Finger Dynamics :

The dynamics of the  $i^{th}$  finger can be written in the form

$$M^i(\theta^i)\ddot{\theta}^i + d^i(\theta^i, \dot{\theta}^i) + (J_f^i)^T F_c^i = \tau^i \quad (3.1)$$

where  $M^i(\theta^i)$  is the positive definite inertia matrix of the finger,  $d^i(\theta^i, \dot{\theta}^i)$  represents the centripetal, Coriolis, friction and gravitational terms,  $J_f^i$  is the Jacobian matrix of the finger,  $F_c^i$  is the fingertip contact force vector, and  $\tau^i$  represents the joint torque vector.

For 3 fingers, with only two joints per finger, equation(3.1) may be aggregated to give

$$M(\theta)\ddot{\theta} + d(\theta, \dot{\theta}) + J_f^T F_c = \tau \quad (3.2)$$

where  $M(\theta) = \text{Diag}(M^1, M^2, M^3)$  is the  $6 \times 6$  combined finger inertia matrix,  $d(\theta, \dot{\theta}) = [d^{1^T} \ d^{2^T} \ d^{3^T}]^T$  is the  $6 \times 1$  vector of centripetal, Coriolis, friction and gravitational terms,  $F_c = [F_c^{1^T} \ F_c^{2^T} \ F_c^{3^T}]^T$  is the  $6 \times 1$  combined vector of finger contact forces, and  $\tau = [\tau^{1^T} \ \tau^{2^T} \ \tau^{3^T}]^T$  is the  $6 \times 1$  combined joint torque vector.

Object Dynamics :

The equations of motion for the object, written about the centre of gravity of the object, can be represented as

$$M_{og}(\tilde{y})\ddot{\tilde{y}} + d_{og}(\tilde{y}, \dot{\tilde{y}}) = G^T F_c + F_{ext} \quad (3.3)$$

where  $\tilde{y} = (p_{cg_x} \ p_{cg_y} \ \psi_{cg_z})$  is the  $3 \times 1$  vector with  $p_{cg_x}, p_{cg_y}$  representing the position vector in x-y plane and  $\psi_{cg_z}$  representing the orientation of the principal coordinate frame located at the centre of gravity in the World Coordinate Frame,  $M_{cg}(\tilde{y}) = \text{Diag}(m_o U, I)$  is the  $3 \times 3$  inertia matrix of the object,  $m_o$  is the mass of the object,  $I$  represents the moment of inertia matrix,  $U$  is the identity matrix,  $d_{cg}(\tilde{y}, \dot{\tilde{y}}) = (-m_o g^T, (\omega \times U \omega)^T)^T$  is the  $3 \times 1$  vector,  $G$  is the Grip Transform matrix,  $F_c$  is the  $6 \times 1$  combined vector of finger contact forces, and  $F_{ext}$  is the external force acting at the centre of gravity of the object. As shown in Fig.(3.1), the position vector  $p_{cg}$  in equation(3.3) can be written in terms of position vector  $p_o$  of the object frame and a  $2 \times 1$  constant vector  $r = (r_x, r_y)^T$  as

$$p_o \equiv p_{cg} + r \quad (3.4)$$

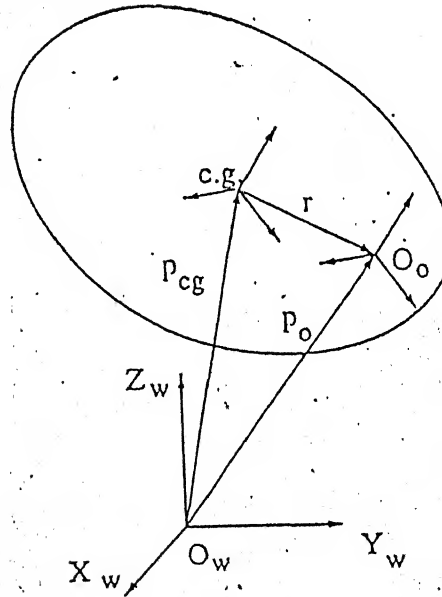


**Figure 3.1 : Representation of a Translated Object Frame.**

Using equation(3.4), equation(3.3) can be written as

$$M_o(y)\ddot{y} + d_o(y, \dot{y}) = G^T F_c + F_{ext} \quad (3.5)$$

where  $M_o = \begin{bmatrix} m_o U & m_o [r] \\ 0 & I \end{bmatrix}$ ,  $d_o = \begin{bmatrix} -m_o g - m_o (\omega \times (\omega \times r)) \\ (\omega \times I \omega) \end{bmatrix}$  and  $[r] = \begin{bmatrix} -r_y \\ r_x \end{bmatrix}$ .

From equations(2.25)-(2.26) and (3.3), the object dynamics can be represented as

$$M_o(\theta) \frac{\partial h_o(\theta)}{\partial \theta} \ddot{\theta} + d_o(\theta, \dot{\theta}) + M_o(\theta) \frac{\partial}{\partial \theta} \left( \frac{\partial h_o(\theta)}{\partial \theta} \dot{\theta} \right) \dot{\theta} = G^T F_c + F_{ext} \quad (3.6)$$

**Finger-Object Dynamics :**

The fingertip contact force vector  $F_c$  can be calculated as

$$F_c = F_p + F_h \quad (3.7)$$

where manipulating force  $F_p$  represents the particular solution and the grasping force  $F_h$  represents the homogeneous solution for the contact force  $F_c$ . The particular solution  $F_p$  denotes the equilibrating forces, solely responsible for balancing the external forces and does not contribute to the grasping forces.  $F_h$  is an arbitrary vector in the null space of the Moore-Penrose inverse  $G^{\#T}$  of the grip transformation matrix  $G^T$ .

From [Kumar, 1988] the combined finger-object dynamics can be written as

$$\hat{M}(\theta) \ddot{\theta} + \hat{d}(\theta, \dot{\theta}) + J_f^T F_h - J_f^T G^{\#T} F_{ext} = \tau \quad (3.8)$$

where  $\hat{M} = \left[ M(\theta) + J_f^T G^{\#T} \left( M_o(\theta) \frac{\partial h}{\partial \theta} \right) \right]$  and

$$\hat{d} = \left[ d(\theta, \dot{\theta}) + J_f^T G^{\#T} \left\{ d_o(\theta, \dot{\theta}) + M_o(\theta) \frac{\partial}{\partial \theta} \left( \frac{\partial h}{\partial \theta} \dot{\theta} \right) \dot{\theta} \right\} \right].$$

### 3.3 Controller Model

Let a matrix  $N_G$  is defined as

$$N_G = (J_f^T)^{-1} \left( \frac{\partial \phi}{\partial \theta} \right)^T \quad (3.9)$$

such that the null space of  $G^T$  is completely spanned by the columns of the matrix  $N_G$  for a force closed grasp.

Then, the vector  $F_h$  can be expressed as

$$F_h = N_G \chi \quad (3.10)$$

where  $\chi$  is an arbitrary vector of dimension  $3 \times 1$  for the planer hand case.

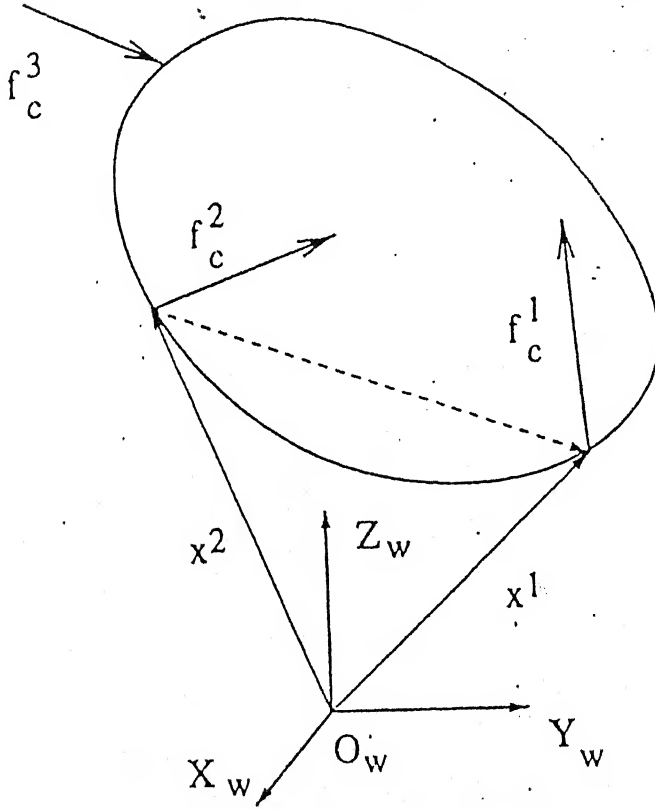


**Figure 3.2 : Defining the Grasping Force Parameter  $\lambda_h$**

Define a linear transformation matrix  $L$  of dimension and  $\text{rank}(L)=3$  for the planer hand case such that  $LF_c$  gives the projection of the difference of the contact forces along the line joining the corresponding contact points. Projection of the difference of the contact forces  $F_c^1$  and  $F_c^2$  can be written from the figure(3.2) as

$$\begin{aligned}
\lambda_{h_1} &= (X^1 - X^2)^T (F_c^1 - F_c^2) \\
\text{or, } \lambda_{h_1} &= \left[ (X^1 - X^2)^T \quad -(X^1 - X^2)^T \right] \begin{bmatrix} F_c^1 \\ F_c^2 \end{bmatrix} \\
\text{or, } \lambda_{h_1} &= L^1 F_c
\end{aligned} \tag{3.11}$$

where  $\lambda_{h_1}$  represents the first grasping force parameter component,  $X^1$  and  $X^2$  are the position of the first and second contact points, respectively, in the World Coordinate Frame  $O_W X_W Y_W Z_W$ . The grasping force parameter  $\lambda_h$  is written as

$$\lambda_h = \begin{bmatrix} \lambda_{h_1}^T \\ \lambda_{h_2}^T \\ \lambda_{h_3}^T \end{bmatrix} \tag{3.12}$$

The linear transformation matrix  $L$  is defined as

$$L = \begin{bmatrix} L^1 \\ L^2 \\ L^3 \end{bmatrix} = \begin{bmatrix} (x^1 - x^2)^* & (y^1 - y^2)^* & -(x^1 - x^2)^* & -(y^1 - y^2)^* & 0 & 0 \\ 0 & 0 & (x^2 - x^3)^* & (y^2 - y^3)^* & -(x^2 - x^3)^* & -(y^2 - y^3)^* \\ -(x^3 - x^1)^* & -(y^3 - y^1)^* & 0 & 0 & (x^3 - x^1)^* & (y^3 - y^1)^* \end{bmatrix} \tag{3.13}$$

where  $(X^i - X^{i+1})^* = (X^i - X^{i+1}) / \|X^i - X^{i+1}\|$

Using equations(3.11) and (3.13), the complete grasping force parameter vector  $\lambda_h$  can be written as

$$\lambda_h = L F_c \tag{3.14}$$

As discussed in [Dasgupta, 1998], we have

$$L F_p = 0 \tag{3.15}$$

Thus

$$\lambda_h = L(F_p + F_h) = L F_h = L N_G \chi \tag{3.16}$$

Let a vector  $z_{15 \times 1}$  is defined such that

$$z = [z_1^T \quad z_2^T \quad z_3^T \quad z_4^T \quad z_5^T]^T \quad (3.17)$$

where  $z_1 = \begin{bmatrix} p_{o_x} \\ p_{o_y} \\ \phi_z \end{bmatrix}$  is the generalized position vector denoting the position and

orientation of object in World Coordinate Frame,  $z_2 = \dot{z}_1 = 0$ ,  $z_3 = \begin{bmatrix} \phi^{12} \\ \phi^{23} \\ \phi^{31} \end{bmatrix} = 0$  is the constraints vector,  $z_4 = \dot{z}_3 = 0$ , and  $z_5 = \lambda_h = LF_c$ . Here  $L$  is the linear transformation matrix,  $F_c$  is the contact force vector and  $\lambda_h$  is grasping force parameter. Also let us define the derivatives of the vector  $z$  such that

$$\begin{aligned} \dot{z}_1 &= z_2 & \dot{z}_2 &= 0 \\ \dot{z}_3 &= z_4 & \dot{z}_4 &= 0 \\ \dot{z}_5 &= w = \dot{\lambda}_h \end{aligned} \quad (3.18)$$

where  $w$  is fictitious input as defined in equation (3.25).

The equation of motion can be written as

$$\tau = \hat{d} + J_f N_G \hat{L} \lambda_h + \hat{M} \Gamma^{-1} \begin{bmatrix} \pi_1^T \\ \pi_2^T \end{bmatrix} - \hat{M} \Gamma^{-1} \begin{bmatrix} \frac{\partial}{\partial \theta} (h \dot{\theta}) \\ \frac{\partial}{\partial \theta} (\phi \dot{\theta}) \end{bmatrix} \dot{\theta} \quad (3.19)$$

where  $\tau$  is the applied joint torque,  $\hat{d} = \begin{bmatrix} 0 \\ 0 \\ -mg \end{bmatrix}$  is the vector of gravity terms [ $m$  = mass of the object],  $J_f$  is the finger Jacobian ( $6 \times 6$ ),  $\lambda_h$  is the grasping

force parameter vector,  $\hat{M} = \begin{bmatrix} 1 & 0 & 0 \\ 0 & 1 & 0 \\ 0 & 0 & 1 \end{bmatrix}$  is the inertia matrix,  $\Gamma = \begin{bmatrix} \left( \frac{\partial h_e}{\partial \theta} \right)^T \\ \left( \frac{\partial \phi}{\partial \theta} \right)^T \end{bmatrix}$  is a

square non-singular matrix,  $\pi = [\pi_1^T \quad \pi_2^T \quad \pi_3^T]^T$  as defined in equations (3.21)-



(3.23),  $\lambda_h$  is the grasping force parameter vector,  $h_o(\theta)$  is the generalized position vector from equations(2.24) and (2.25), and  $\phi$  represent constraints. Here  $\hat{L}$  is defined as following

$$\hat{L} = (LN_G)^{-1} \quad (3.20)$$

### 3.3.1 State Feedback Controller

New input vector  $\pi = [\pi_1^T \ \pi_2^T \ \pi_3^T]^T$  is expressed in terms of vector  $z = [z_1^T \ z_2^T \ z_3^T \ z_4^T \ z_5^T]^T$  as following

$$\pi_1 = \dot{z}_{2d} - K_{1p}(z_1 - z_{1d}) - K_{1v}(z_2 - z_{2d}) \quad (3.21)$$

$$\pi_2 = \dot{z}_{4d} - K_{2p}(z_3 - z_{3d}) - K_{2v}(z_4 - z_{4d}) \quad (X3.22)$$

$$\pi_3 = \dot{z}_{5d} - K_f(\hat{\lambda} - z_{5d}) \quad (3.23)$$

where subscript- $d$  denotes desired reference values,  $K_{1p} = \text{Diag}(K_{1p}^1 \ K_{1p}^2 \ K_{1p}^3)$ ,  $K_{1v} = \text{Diag}(K_{1v}^1 \ K_{1v}^2 \ K_{1v}^3)$ ,  $K_{2p} = \text{Diag}(K_{2p}^1 \ K_{2p}^2 \ K_{2p}^3)$ ,  $K_{2v} = \text{Diag}(K_{2v}^1 \ K_{2v}^2 \ K_{2v}^3)$  and  $K_f = \text{Diag}(K_f^1 \ K_f^2 \ K_f^3)$  are positive definite gain matrices, and  $\hat{\lambda}_h$  is the feedback of the grasping force parameter vector.

The overall controller for the closed loop system can be written as

$$\tau = \hat{d} + J^T N_G \hat{L} \lambda_h + \hat{M} \Gamma^{-1} \left[ \begin{pmatrix} \dot{z}_{2d}^T \\ \dot{z}_{4d}^T \end{pmatrix} - \frac{\partial}{\partial \theta} (\Gamma \dot{\theta}) \dot{\theta} - \begin{bmatrix} K_{1p} & 0 \\ 0 & K_{2p} \end{bmatrix} \begin{bmatrix} (z_1 - z_{1d})^T \\ (z_3 - z_{3d})^T \end{bmatrix} - \begin{bmatrix} K_{1v} & 0 \\ 0 & K_{2v} \end{bmatrix} \begin{bmatrix} (z_2 - z_{2d})^T \\ (z_4 - z_{4d})^T \end{bmatrix} \right] \quad (3.24)$$

$$w = \pi_3 = \dot{z}_{5d} - K_f(\hat{\lambda}_h - z_{5d}) \quad (3.25)$$

The desired trajectory of the object, in terms of the position, velocity and acceleration of the object, is specified through  $z_{1d}, z_{2d}$  ( $\dot{z}_{1d}$ ) and  $\dot{z}_{2d}$  ( $\ddot{z}_{1d}$ ) in equation(3.21). For the constraints to be satisfied, the desired values of  $z_{3d}, z_{4d}$  ( $\dot{z}_{3d}$ ) and  $\dot{z}_{4d}$  ( $\ddot{z}_{3d}$ ) are specified in equation(3.22). The desired trajectory of the grasping force parameter vector is specified through  $z_{5d}$  and  $\dot{z}_{5d}$ .

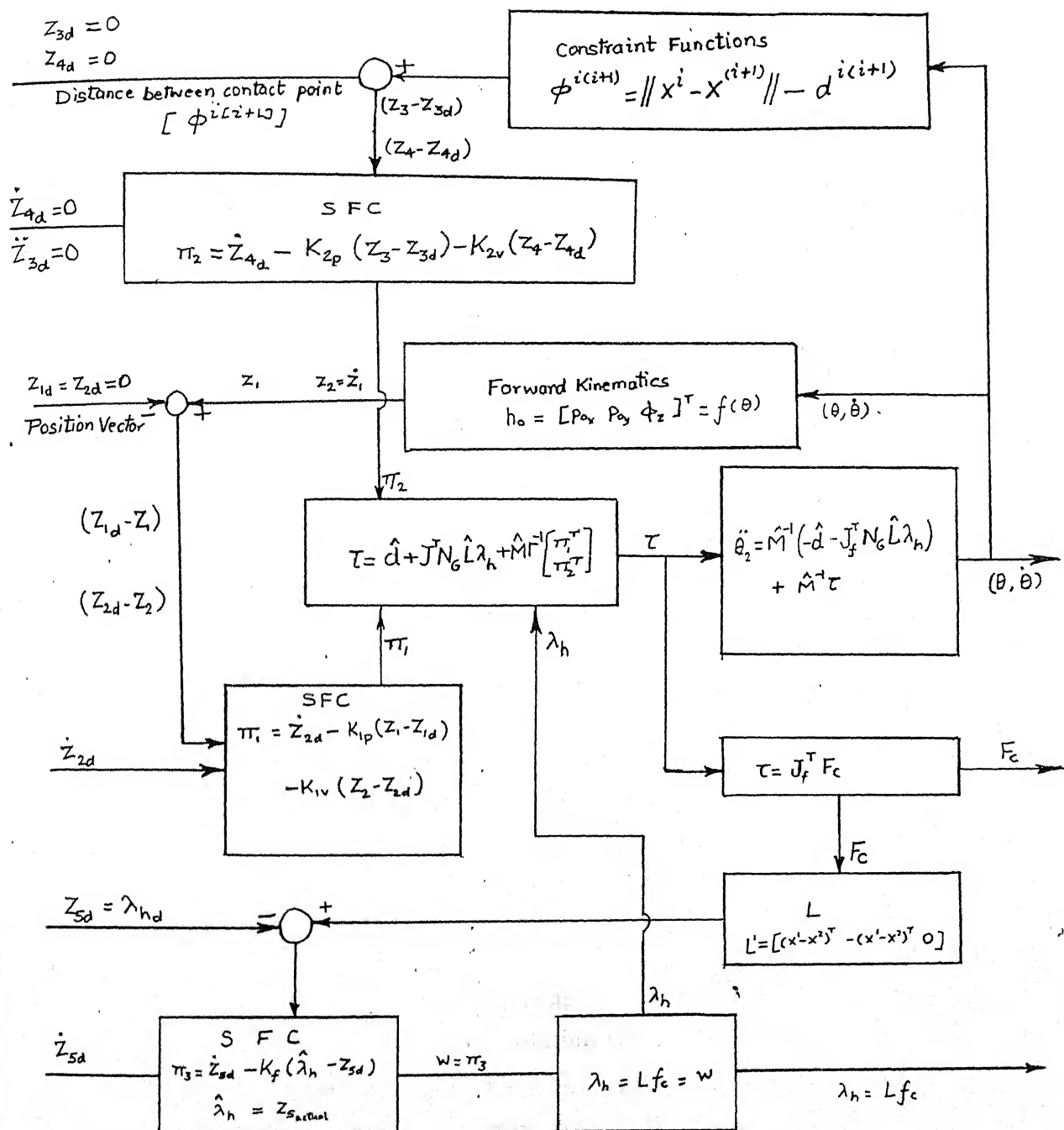


Figure 3.3 : Block Diagram for the Closed-loop Control

The feedback of the grasping force parameter vector  $\hat{\lambda}_h$  in equation(3.23) is obtained from the measurement of the finger contact force  $F_c$ . From the equation(3.16)  $\hat{\lambda}_h$  could be written as

$$\hat{\lambda}_h = LF_c \quad (3.26)$$

### 3.4 Control of Grasping Force

For a typical contact situation at  $i^{th}$  fingertip, where the contact force  $F_c^i$  is applied at the point of contact and  $C_n^i$ ,  $C_t^i$ , respectively, represent the component of the contact force along the contact normal and tangential force; the condition for stability of the contact at the point of contact can be written as

$$\mu_i \|C_n^i\| - \|C_t^i\| \geq 0 \quad (3.27)$$

where  $\mu_i$  is the coefficient of friction for fingertip-object contact.

Above relation represents a convex cone, known as friction cone. Grasp is stable [Bicchi, 1995] if, at each contact point, the contact forces are within the corresponding friction cone.

The significance of the equation(3.27) is that the net force at any contact point must satisfy this equation. The net force  $F_c$  at any contact point can be decomposed into two components [as mentioned in equation(3.7)], namely, the particular solution giving the equilibrating force [or manipulation force]  $F_p$ , and the homogeneous solution giving the grasping force  $F_h$ . Equilibrating force [manipulating force]  $F_p$  is determined by the external and dynamic forces on the object and can not be specified independently; whereas grasping force  $F_h$  can be specified independently.

A stable grasp can be obtained; if there exists a grasping force vector  $F_h$  such that, for a grasp with  $F_c = F_h$  and no external force on the object, equation(3.27) is satisfied at all contact points by appropriately scaling the grasping force vector  $F_h$ .

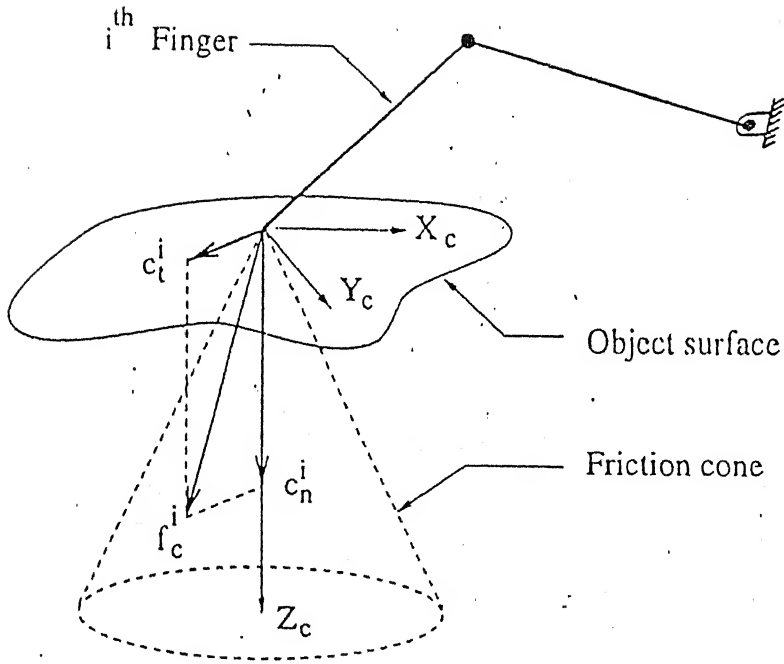


**Figure 3.4 : Schematic Representation For a Typical Contact Case**

### 3.4.1 Optimal Grasping Strategy

Formulating the optimization problem

$$\begin{aligned}
 \text{Min} \quad & f_g = c_1 F_c^T F_c - c_2 F_c^T \hat{n} \\
 \text{subject to} \quad & G^T F_c = F_o
 \end{aligned} \tag{3.28}$$

where  $c_1$  and  $c_2$  are appropriate constants for normalization of the terms  $F_c^T F_c$  and  $F_c^T \hat{n}$ , respectively, in the objective function  $f_g$ ,  $F_c$  is the contact force vector,  $\hat{n}$  is the unit surface normal vector,  $G$  is the Grip Transform Matrix, and  $F_o$  is the external force applied on the object at the origin of the object frame. The term  $F_c^T F_c$  is the squared norm of the contact forces. The term  $F_c^T \hat{n}$  is the sum of the projection of the contact forces along the corresponding contact normals, since it has a negative sign, the minimization of  $f_g$

maximizes the sum of the projections of the contact forces along the corresponding contact normals. The increase of the contact forces  $F_c$  due to maximization of the sum of the projections of the contact forces along the corresponding contact normals is taken care of by the minimization of the squared norm  $F_c^T F_c$  of the contact forces.

Writing the augmented cost function of the equation(3.28), we have

$$f_{aug} = c_1 F_c^T F_c - c_2 F_c^T \hat{n} + \lambda^T (G^T F_c - F_o) \quad (3.29)$$

where  $f_{aug}$  is the augmented cost function and  $\lambda$  is the Lagrange multiplier. From the necessary conditions of optimality

$$\left. \frac{\partial f_{aug}}{\partial F_c} \right|_{(F_c^*, \lambda^*)} = 0 \quad \text{and} \quad \left. \frac{\partial f_{aug}}{\partial \lambda} \right|_{(F_c^*, \lambda^*)} = 0 \quad (3.30)$$

we have

$$F_c^* = \frac{1}{2} G^{\#T} F_o + P \hat{n} \quad (3.31)$$

where  $G^{\#T}$  is the Moore-Penrose inverse [Rao, 1971] of  $G^T$ ,  $I$  is the identity matrix, and  $P = -\frac{1}{2} c_1^{-1} c_2 (I - G^{\#T} G^T)$ .

As we have

$$F_p = G^{\#T} F_o, \quad (3.32)$$

it can be written from equations (3.31) and (3.32) as

$$F_c^* = F_p + P \hat{n} \quad (3.33)$$

The closed form optimal solution for  $F_c$  gives the optimized value of the grasping force  $F_h$ , since  $F_p$  is fully dependent upon external forces.

### 3.4.2 Grasping Force Considerations

The grasping force controller as given in equation(3.16) requires the specification of the desired force parameter vector  $z_{sd}$ . Since  $F_h = N_G \hat{L} \lambda_h$  and  $\lambda_h = z_5$ , the desired optimal force parameter vector  $z_{sd}^*$  can be obtained from

$$\begin{aligned} N_G \hat{L} z_{sd}^* &= P \hat{n} \\ \text{or, } z_{sd}^* &= \hat{L}^{-1} (N_G^T N_G)^{-1} N_G^T P \hat{n} \end{aligned} \quad (3.34)$$

when some external force is present, i.e.,  $F_p \neq 0$ .

Define a scaling law for the grasping force parameter  $z_{sd}^*$  as

$$\begin{aligned} z_{sd} &= (1 + z_6) z_{sd}^* \\ \dot{z}_{sd} &= z_7 z_{sd}^* \end{aligned} \quad (3.35)$$

where  $(z_6, z_7)$  are the states of a second order dynamical system [Dasgupta, 1998] which result in a smooth scaling of  $z_{sd}$  and  $\dot{z}_{sd}$ .

In nutshell, using equation(3.33), optimal grasping force vector  $F_h^*$  is scaled such as to stabilize the grasp.

A norm function  $\alpha$  can be defined such as to measure the distance of any grasp from the good grasp.

For  $i^{th}$  contact point, the cosine of the friction angle (c.f.a.)  $\alpha^i$  can be defined as

$$\alpha^i = \frac{(\hat{n}^i)^T F_c^i}{\|F_c^i\|} \quad (3.36)$$

where  $\hat{n}^i$  is the  $2 \times 1$  unit normal vector on object surface and  $F_c^i$  is the contact force at the  $i^{th}$  contact point. The numerical value of  $\alpha^i$  can be changed by changing  $F_h$  (as changing  $F_h$  changes  $F_c$ ). The optimal c.f.a. vector

$\alpha^* = [\alpha^{1*} \quad \alpha^{2*} \quad \alpha^{3*}]^T$  is the c.f.a. vector [Chung, 1993] at all the contact points for  $F_c = F_h^*$  (*i.e.*,  $F_p = 0$ ). Since c.f.a.  $\alpha^*$  corresponds to a stable grasp, any  $\alpha > \alpha^*$  will definitely yield a stable grasp.

# Chapter 4

## Design Details

---

### 4.1 Introduction

Design is a multistep process which begins with a description of the range of tasks to be performed. Several viable alternative configurations are then determined, followed by an evaluation of the configurations with reference to the sizing of components and dynamic system performance based on appropriate technical and economic criteria, a configuration is then selected. If no configuration meets the criteria, the process may be repeated in an iterative manner until a configuration is selected [Nof, 1985].

In the present chapter design scheme and dimensions are given for finger links and base plate. Criteria for selection of motor/power drive is also discussed. Strain gauges are used to measure the force applied at the fingertip and the scheme for the circuitry involved is discussed.



## 4.2 Finger Design

The planar hand consists of three fingers. Each finger has two links with revolute joints and thus each finger has two degrees of freedom. Joint axes are all parallel and thus the fingertips can move in a single plane as shown in Fig (4.1).

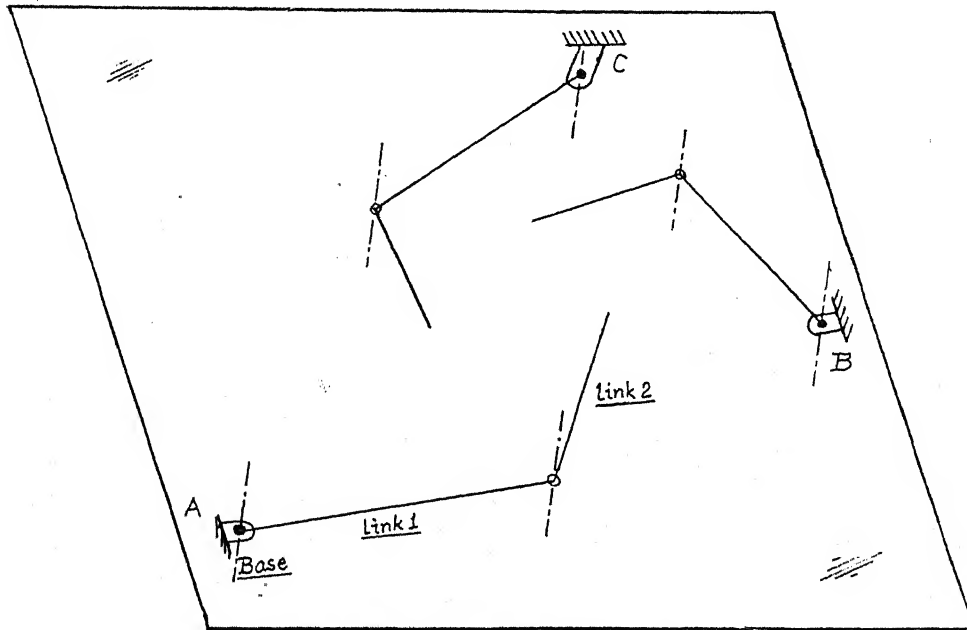


Figure 4.1 : Planar Hand Joint Axes Schematic.

The planar hand [McDonald, 1986] is having total six degrees of freedom. The grasped object [Crossley, 1977] is taken to be having three degrees of freedom in the task space namely, one rotational degree of freedom in the plane perpendicular to the joint axes and two translational degrees of freedom in the plane perpendicular to the joint axes. If we take joint axes parallel to the  $z$ -axis of the World Coordinate Frame, the translational motion will be in the  $x$ - $y$  plane of the World Coordinate Frame. Thus the position and orientation of the object in World Coordinate Frame can be defined by position vectors  $p_{ox}$ ,  $p_{oy}$ , and the orientation vector  $\psi_z$  as presented in the equation (2.25) and as shown in Fig.(4.2).

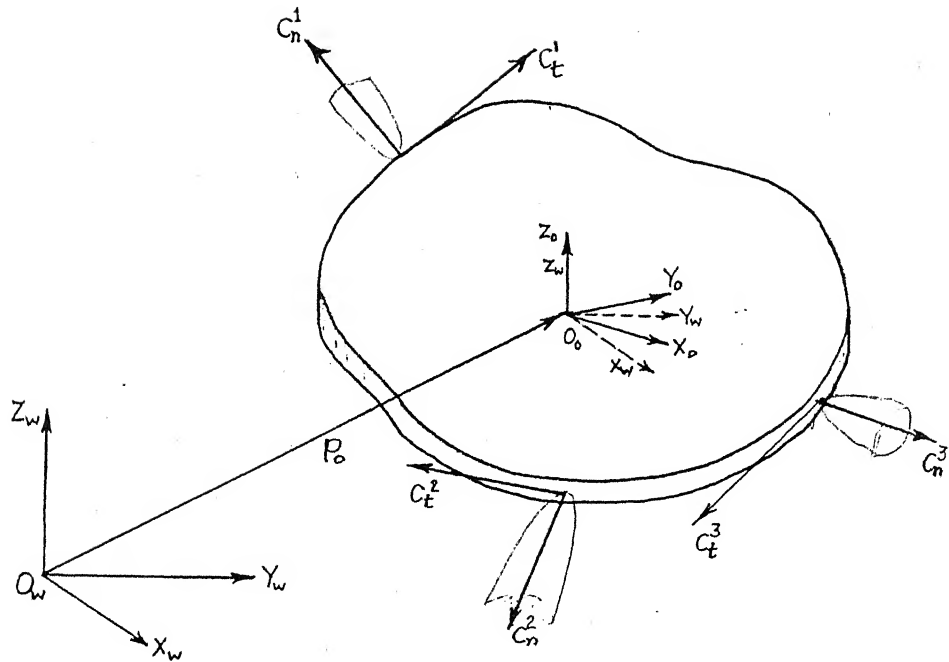


Figure 4.2 : Object Position and Orientation Schematic.

### Material Selection :

The material for the links is selected on the basis of stiffness-to-weight ratio [Rivin, 1988], high strength and low weight. To increase the stiffness-to-weight ratio, the increase in the elastic modulus  $E$  is very desirable, if it is not accompanied by an unacceptable increase in specific density  $\rho$ . Parameters of some high modulus and/or low specific density materials are discussed in [Rivin, 1988]. Best properties are demonstrated by ceramics (boron carbide and aluminium) and beryllium. While ceramics are brittle and difficult to machine, beryllium is very costly, Fiber reinforced materials also have good stiffness-to-weight ratio but their applications are limited because of creep under constant load (for some compositions), aging, high thermal expansion coefficient, difficulty of joining with metal parts and high cost. Popular light structural materials as magnesium, aluminium and titanium have the same  $E/\rho$  ratios as that of steel [Andeen, 1988]. Thus these materials are used where low weight with high strength is more important than  $E/\rho$  ratios.

Thus considering all these factors aluminium is selected as material for the links.

### Basic Link Features :

The link dimensions are taken so as to minimize the link weight, deflection under loading and to maximize the force generated at the end of the link. The scheme for finger links arrangement is shown in figure (4.3).

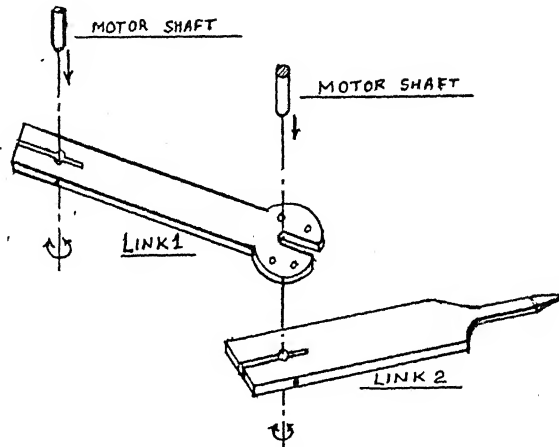


Figure 4.3 : Finger Links Arrangement Schematic.

The big end of link-1 is slotted such as to provide ease in assembly. With this arrangement the motor can be fixed to link-1 end and then link-2 can be connected to its shaft or vice-versa as shown in Figure (4.4).

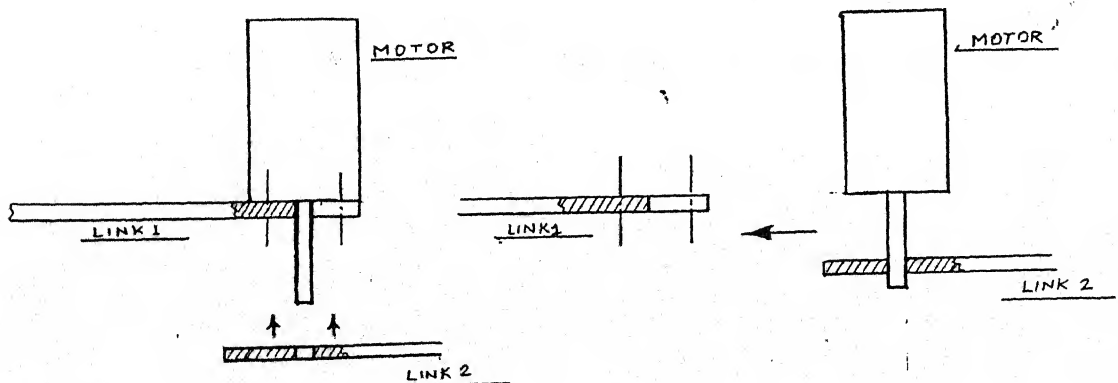


Figure 4.4 : Link Assembly Schematic.

The small end of link-1 and big end of link-2 is slitted and a screw hole is provided as shown in Fig.(4.5). This provision offers a means to clamp the shaft and provide ease in assembly and disassembly.

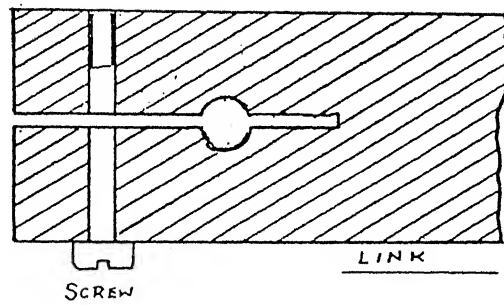


Figure 4.5 : Provision for Clamping of Shaft.

The small end in link-2 is kept pointed. The cross-sectional dimensions of link-2 are reduced so that when some force is applied at the fingertip there is a measurable deflection in that part. Strain gauges are mounted on the narrow part of the link to measure the deflection. The schematic is shown in Fig(4.6).

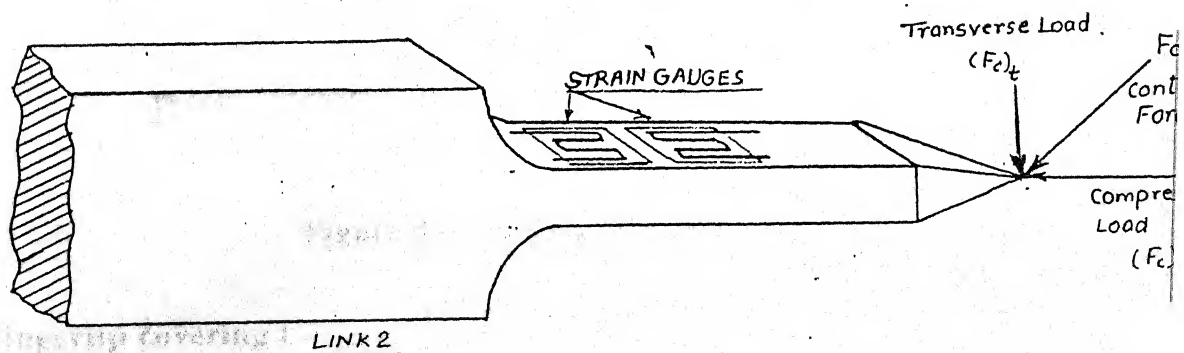


Figure 4.6 : Strain gauge Mounting Schematic.

The detailed dimensions for both links are given in Figs.(4.7) and (4.8).

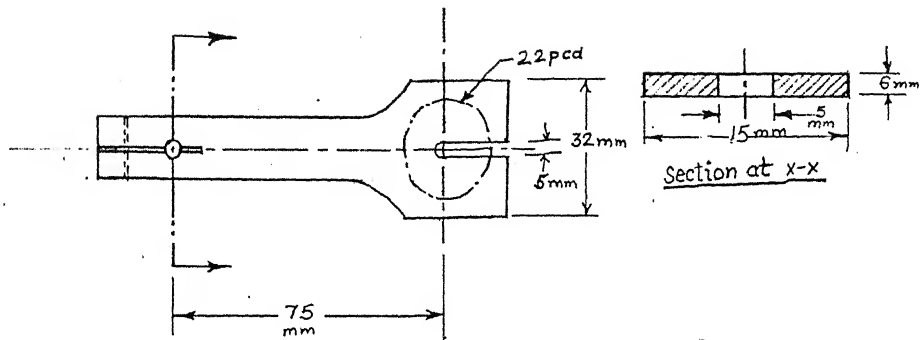
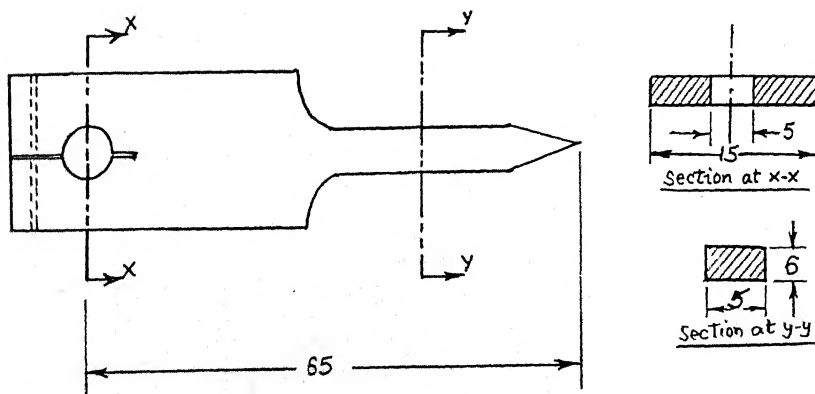


Figure 4.7 : Link-1 Dimensions.



[All Dim.in mm]

Figure 4.8 : Link-2 Dimensions.

#### Fingertip covering :

Fingertip covering is made of light rubber in order to increase the friction between the fingertip and the object at the contact point. Fingertip schematic is shown in Fig.(4.9).

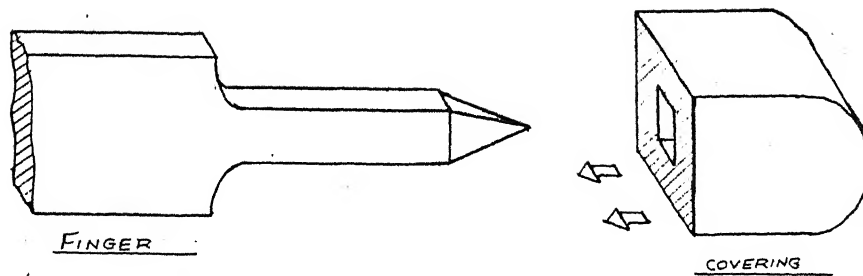


**Figure 4.9 : Fingertip Covering Schematic.**

#### **Finger Mounting :**

The finger mounting is provided to fix the finger on the base plate. It is fastened by a screw on the plate. Aluminium is taken as the material.

The overall arrangement for the setup is shown in the Fig.(4.10).

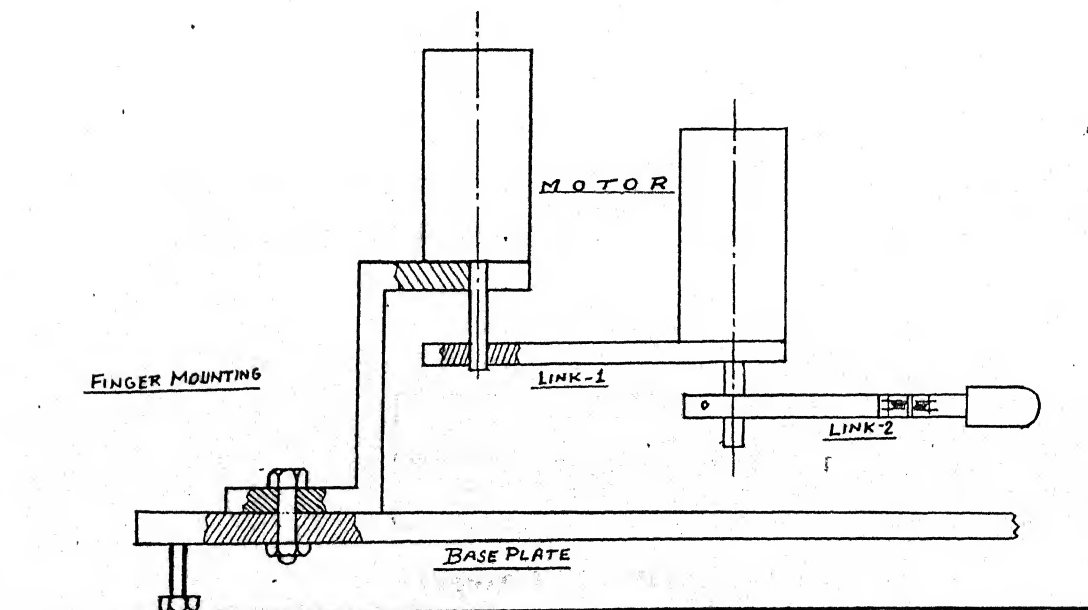


**Figure 4.10 : Overall Finger Arrangement.**

### Base Plate :

Base Plate is provided to mount the fingers. Cast iron is taken as base plate material due to its low cost. Four screws are provided to adjust the level of the base plate. Slots are provided in the base plate, as shown in Fig.(4.11), to adjust the relative position of the finger bases. In the design of the base plate, size and arrangement of the links are taken into account. The ease of arbitrarily changing the position and orientation of the fingertips is taken into account. As shown in [Yoshikawa, 1990], the best configuration in terms of manipulability is achieved when the angle between the link-1 and link-2 is approximately 90 degrees.

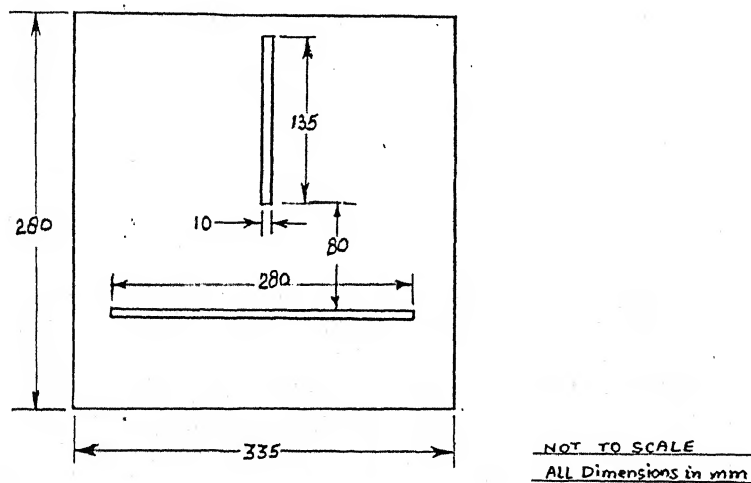


Figure 4.11 : Base Plate Dimensions.

### Object :

The object is made of perspex sheet. It is of cylindrical shape and made hollow to reduce the weight. Dimensions of the object are shown in Fig.(4.12).

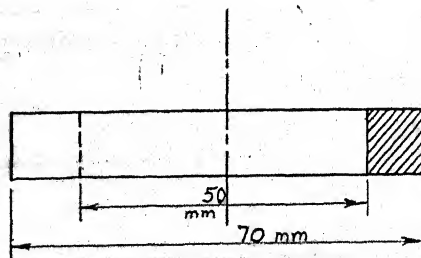


Figure 4.12 : Object Dimensions.

The top view of the actual setup is shown in Fig.(4.13).

### 4.3 Motor Selection and Specifications

The motors required to move the fingers of the planar hand must be having high torque-to-weight ratio[Asada, 1987]. Also the motors should not be very costly. DC servo motor with encoder facility is a suitable choice. The DC motor used is having an ironless rotor combined with a commutation system containing a graphite copper combination for the brushgear. The active rotor part simply consists of cylindrical skew winding and requires no support. Because of the absence of an iron core rotor inertia is very low. This very low value of inertia allows for increased rates of acceleration and deceleration and also provides optimum performance under conditions of shock and vibration. The basic features of the motor are given in Table 4.1.

Features	Benefits
Capability of commutating high current densities	High peak torques with no risk of demagnetizing the stator. Very long life.
155 degree Celsius rated motor temperature	Exceptionally high continuous torque for the motor size. Savings in weight, space, and cooling equipment.
Commutation system of compact construction	Excellent resistance to severe conditions of shock and vibration.
High torque-to-inertia ratio	High acceleration, short mechanical time constant.
Robust graphite-copper commutation system	High peak currents for fast incremental motion. Very long life in drive and servo systems.
Low rotor inertia	High acceleration, excellent resistance to shocks and vibration.

**Table : 4.1 Basic Features of the Motor Used.**



There are no preferred rotor position at stall condition because of absence of iron. The rotor is able to stop in any position due to low rotor inertia. Motor running speed is not limited by iron losses but depends only on supply voltage and load torque. Motor stator part consists of a cylindrical two-pole permanent magnet that fits inside a steel tube closing the magnet circuit. The selected motor is of very low inductance and they need a relatively low current  $I$  for a given torque. Arcing during commutation which is approximately proportional to  $I^2L$  is therefore much smaller than with conventional DC motors. The powerful magnet surrounded by the winding generates a strong induction in the air gap. Together with an optimum copper volume, power output for a given motor size and weight is exceptionally high. The motor specifications are given in Table (4.2).

Make	<i>escap</i> ® 35NT2R82-426SP
No. of motors used	6
Measuring voltage	32 V
No-load speed	6100 rpm
Stall torque	720 mNm
Average no-load current	80 mA
Maximum continuous current	2.3 A
Maximum recommended speed	9000 rpm
Maximum angular acceleration	$64 \times 10^3 \text{ rad/sec}^2$
Maximum continuous output power	75 W
Back-EMF constant	5.2 V/100 rpm
Rotor inductance	0.4 mH
Motor regulation $\frac{R}{k^2}$	$0.89 \times 10^3 / Nms$
Thermal resistance	2.2 ohm
Torque constant	49.7 mNm/A
Rotor inertia	$71.4 \times 10^{-7} \text{ kg m}^2$
Mass of the motor	310 gms.
Mechanical time constant	5.2 ms
Thermal time constant	rotor 60 sec stator 920 sec

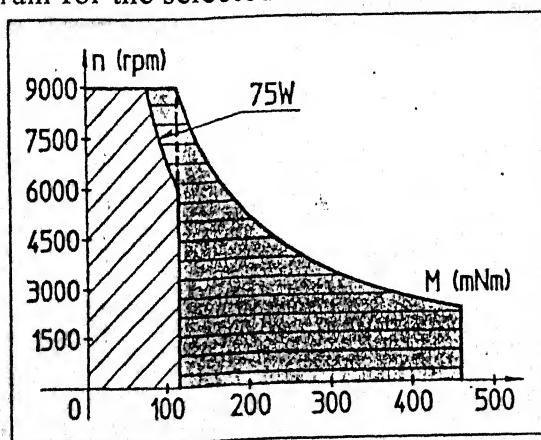
Thermal resistance	rotor-body	3.5 deg.C/W
	body-ambient	8 deg.C/W
Axial play		negligible
Radial play		negligible
Shaft runout		$\leq 10\mu m$
Maximum side load at 10 mm from mounting face ball bearing		35 N
Maximum permissible coil temperature		155 deg.C
Maximum axial static force for	press-fit	100 N
	shaft-supported	1000 N
Recommended ambient temperature range		-10 deg.C to +80 deg.C

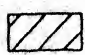
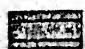
\*GRAPHITE BRUSHES AND COPPER COMMUTATOR WITH 13 SEGMENTS.

\*\*MOTOR IS FITTED WITH TWO PRELOADED BALL BEARINGS.

**Table 4.2 : Important Motor Specifications.**

Speed Torque diagram for the selected motor is shown in the Fig.(4.14).



-  Continuous working range
-  Temporary working range

**Figure 4.14 : Motor Operating Range.**

The speed torque diagram indicates the maximum recommended values of speed, torque and power for both continuous and intermittent operation. The motor dimensions are shown in Fig.(4.15).

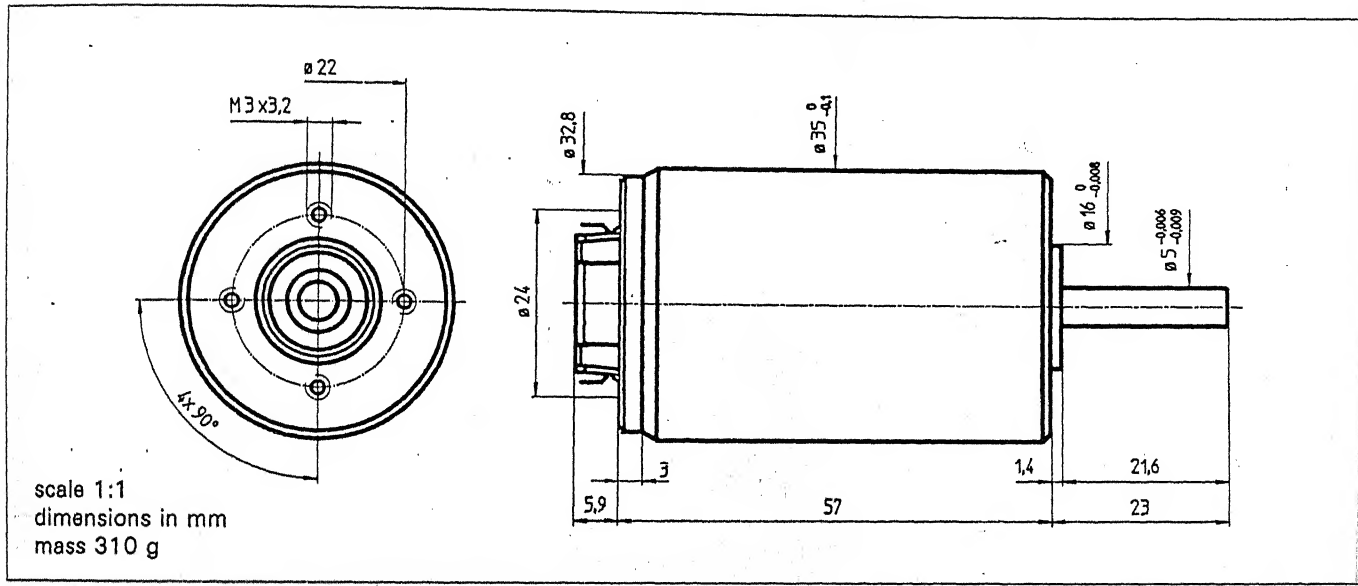
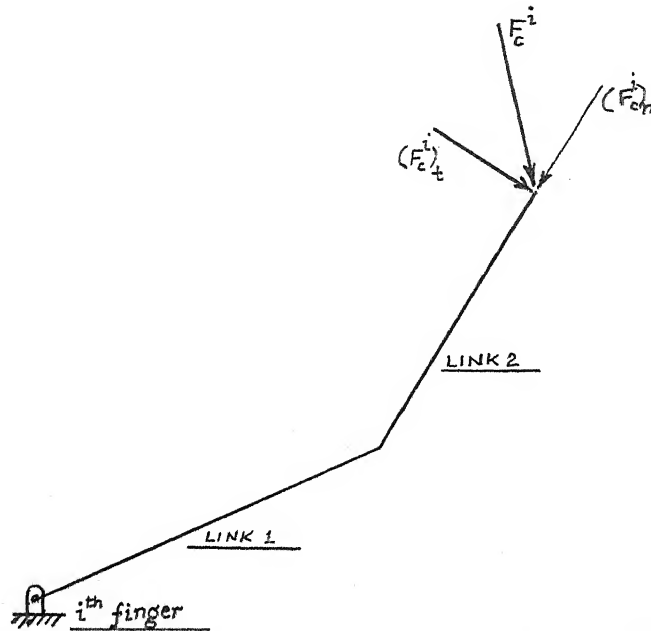


Figure 4.15 : Dimensions for the Selected Motor.

## 4.4 Force Sensing using Strain Gauges

P-type semiconductor strain gauges [Hahm, 1988] are used to measure the deflection in the finger due to force applied at the fingertip. The contact force  $F_c$  is resolved into two components as shown in Fig.(4.16). One component  $(F_c)_n$  is taken along the link and other component  $(F_c)_t$  is taken normal to the link. Wheatstone half bridge [Klafter, 1989] is used as shown in Figs.(4.17) and (4.18). To measure force  $(F_c)_t$  the Wheatstone bridge arrangement as shown in Fig.(4.17) is used. The force  $(F_c)_t$  produces bending stress in the finger, whereas the force  $(F_c)_n$  produces compressive stress on

the finger link. The arrangement for measurement of the force  $(F_c)_n$  is shown in Fig.(4.18).



**Figure 4.16 : Resolving the Components of the Contact Force  $F_c$ .**

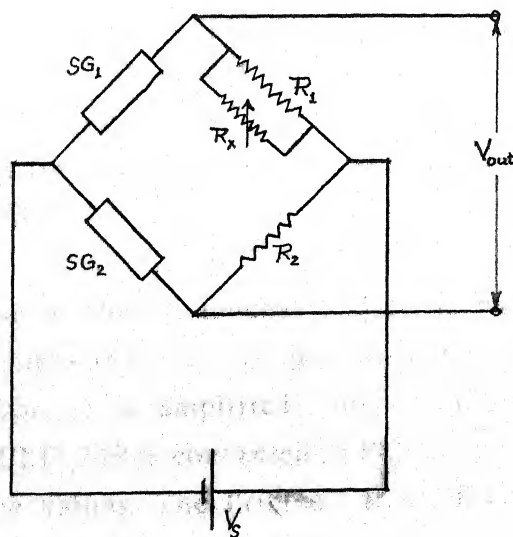


**Figure 4.17 : Wheatstone Bridge Arrangement for measurement of  $(F_c)_t$ .**

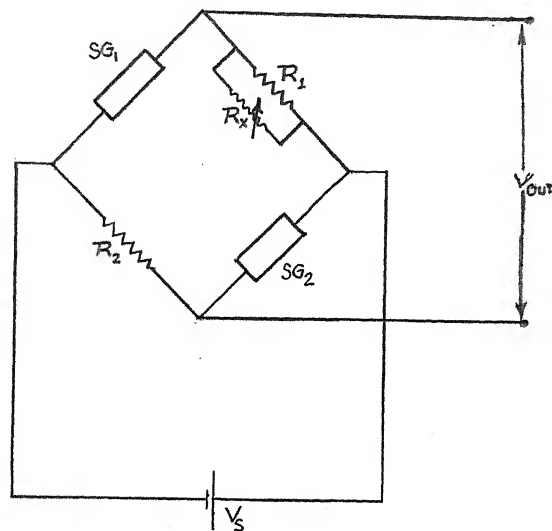
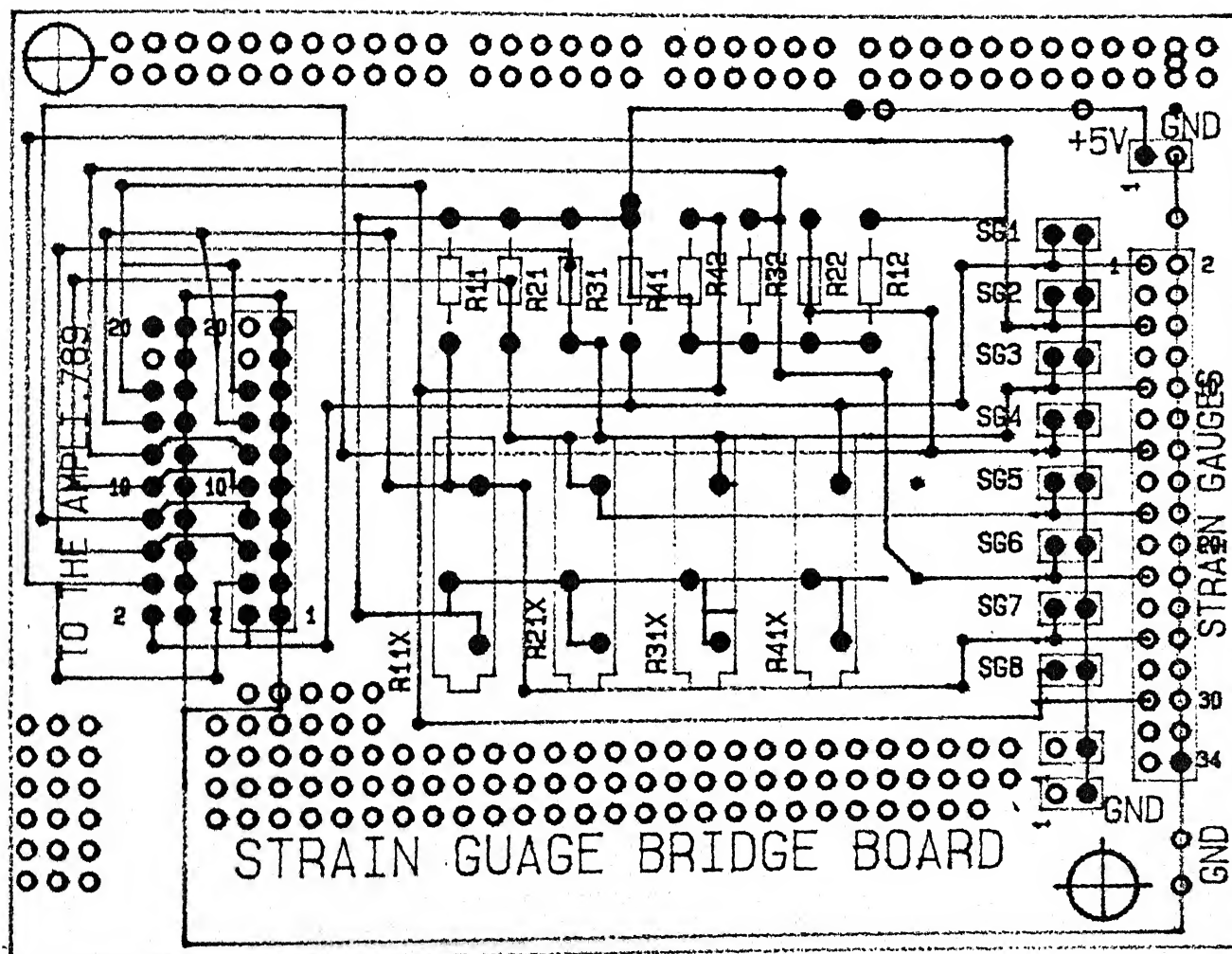


**Figure 4.18 : Wheatstone Bridge Arrangement for measurement of  $(F_c)_n$ .**

The half bridge is balanced when there is no load on the finger tip. Potentiometer resistance is used to adjust the bridge output to zero when gauges are not strained. The values of balancing potentiometer and resistor  $R_1$  in parallel are chosen so that the output voltage may be raised or lowered, since the initial imbalance could have either polarity. A single potentiometer could also be used instead of parallel combination but the resolution will be very poor and fine adjustments to balance the bridge for no-load conditions will be very difficult.

As soon as the tip touches and starts pushing the object the finger deflection changes the strain gauge resistance which unbalances the bridge. The output voltage is amplified using a PCLD-789 amplifier/multiplexer board. The PCLD-789 is connected to PC and a software reads the amplified output voltage values. The Printed Circuit Board (PCB) diagram for half bridge for measuring transverse force is shown in Fig.(4.19).



4.19 PCB diagram for measurement of  $(F_c)_i$

Complete schematic for the force feed back is shown in Fig.(4.20).

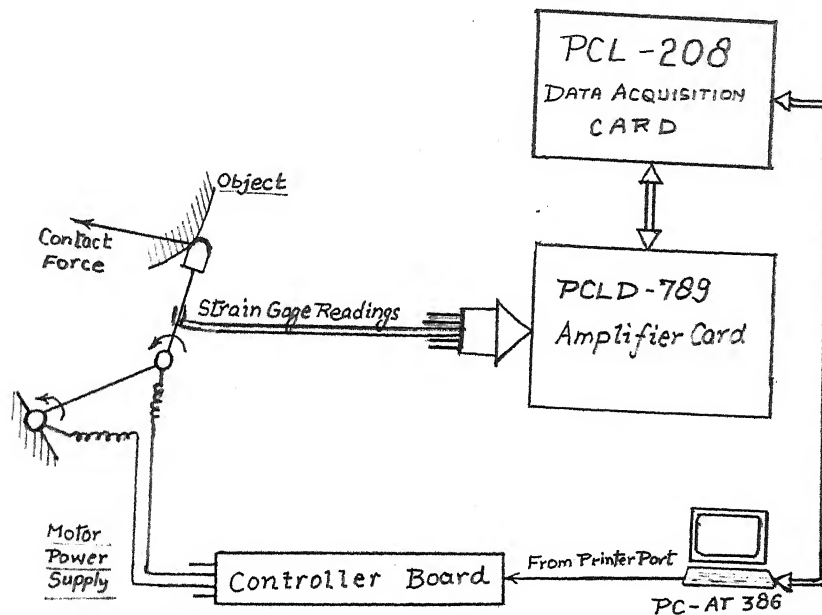


**Figure 4.20 . Force Feedback Schematic.**

The specifications for the selected strain gages are given in Table 4.3.

Type	p-type semiconductor strain gage
Lot tolerance resistance	$300 \pm 10 \% \text{ ohm}$
Gage factor	100
Effective gage length	$< 5 \text{ mm}$
Effective gage width	$< 0.25 \text{ mm}$
Effective gage thickness	$0.025 \text{ mm}$
Overall size	$8 \text{ mm} \times 6 \text{ mm}$
Base material	Phenolic encapsulation

**Table 4.3 : Strain Gauge Specifications.**

## Chapter 5

# Implementation, Results and Discussions

---

### 5.1 Strain Gauge Calibration

Strain gauges form part of the Wheatstone bridge circuit which is kept balanced for no-load-at-fingertip condition by adjusting the potentiometer resistance value. When some external force is applied at the fingertip, the finger is deflected and thus the resistance of the strain gauges changes. This change in the resistance causes unbalances in the Wheatstone bridge. Thus the output voltage changes from zero to some finite value. We can apply some known force at the fingertip and then the output voltage value could be read. Thus the chart for the force and the corresponding output voltage value can be prepared. The same chart can be used to read the force value if the output voltage value is known. Thus the fingertip is calibrated for the force applied and corresponding output voltage.

The calibration chart for the transverse load only, is as shown in Table (5.1).



Mass attached at fingertip (gms)	Output voltage shown on the screen	Mass attached at fingertip (gms)	Output voltage shown on the screen	Mass attached at fingertip (gms)	Output voltage shown on the screen
10	1	110	9	210	18
20	2	120	10	220	19
30	3	130	12	230	19
40	4	140	12	240	20
50	5	150	13	250	20
60	5	160	13		
70	6	170	14		
80	7	180	15		
90	8	190	16		
100	8	200	17		

**Table 5.1 : Calibration Chart for Strain Gauges.  
(Only for the transverse load.)**

The chart is same for all three fingers as the gage factor and the other properties for all strain gages are same. We can also show the results of the calibration in a graph as shown in Fig.(5.1).

पुरुषोत्तम काशीनाथ केलकर पुस्तकालय  
भारतीय प्रौद्योगिकी संस्थान कानपुर

अवधि क्र० A-141996

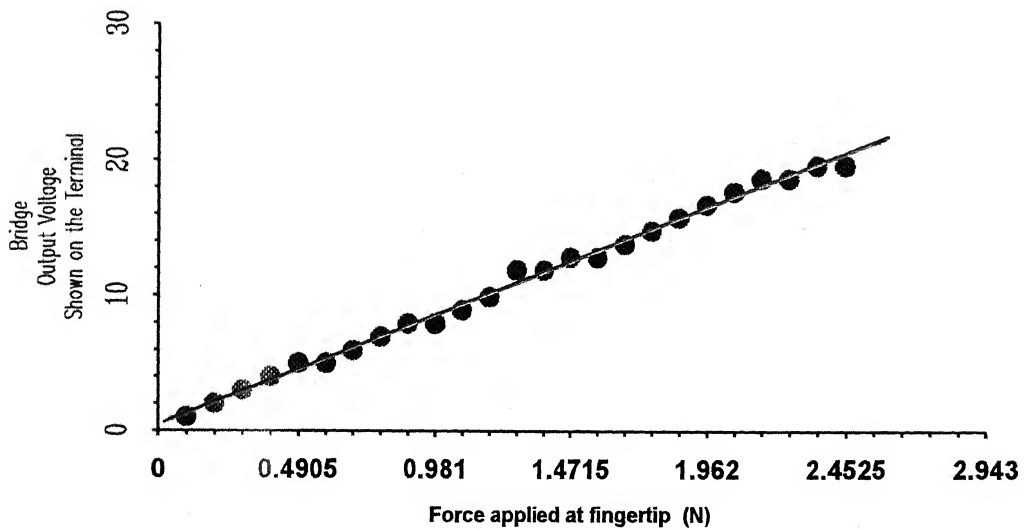


**Figure 5.1 : Graphical Representation of Calibration Results**

## 5.2 Amplification of Bridge Output

Strain gauges are connected to the Wheatstone half bridge PCB to complete the bridge. The complete bridge circuit is as shown in Fig.(5.2).

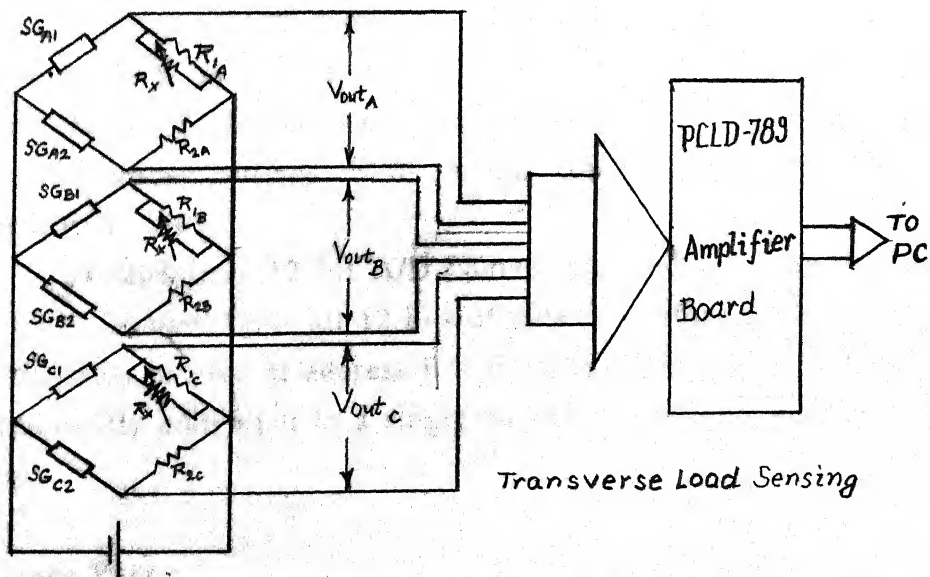


**Figure 5.2 : Output Voltage Amplification Schematic**

### **PCLD-789 (Amplification / Multiplier Board) :**

Analog to digital conversion of the differential voltage of the Wheatstone bridge is carried out inside the PC-AT 386 using PCL-208 card, which is a standard PCB series data acquisition card. However, it requires voltage signals in a particular range to be applied to the input channels of the ADC cards. The differential voltage from the bridge is of very small value, thus the signal needs to be amplified before it can be fed to the input channel of the PCL-208 ADC card. Amplification of the differential input signal is done through the PCLD-789 card, which has instrumentation amplifiers with a range of gain selection. We take the gain of 1000. The amplification is noise free.

The PCLD-789 has 16 differential inputs, out of which first three are used to read the output of three pairs of strain gauges for three fingers. The channel selection is done through the PCL-208 card, which is used for interfacing. All software requirements are dictated by the PCL-208 ADC card. PCLD-789 does not take part in any other software manipulations except for multiplexing the desired channels and connecting the selected input to the output.

### **PCL-208 (Data Acquisition Card) :**

The PCL-208 card is used for analog to digital conversion (ADC) and data acquisition. The card supports 16 single ended or 8 differential analog input configurations. As the PCLD-789 card output is a single ended signal, we use the  $\pm 5$  V single ended input range. This is switch selectable, using different jumper settings. More details could be seen from the Owners Manual PCL-208.

PCL-208 uses 12 bit A/D conversions and an 8 bit register is not enough to accommodate all 12 bits of data. Therefore A/D data is stored in two registers located at address BASE +0 and BASE +1. Through software we can easily convert it to a single number to refer to a particular voltage output.

### **Software Part :**

PC-AT 386 uses vectored interrupts. Whenever a device interrupts the processor, it is responsible for telling the CPU which interrupt service

routine should be executed. The software for interacting and control make use of the vectored interrupts. In order to obtain a real time signal, the timer tick interrupts of PC-AT 386 is used. The timer tick interrupt at vector 1C Hex comes 18.2 times per second. This is because the standard bus clock signal of 2.38 MHz is first divided by 2 and then by  $(2^{16}-1)$ , as the divisor latch (internal to the clock) is loaded by  $(2^{16}-1)$ . Since this rate of timer tick interrupt is too small, the divisor latch is loaded by the software with decimal 256 to obtain exactly 4648 real time interrupts per second. All events, sampling, delays etc., are subsequently timed by this clock.

Force feed back is through the strain gauges mounted at the base of the finger links. The complete A/D operation for reading the differential voltage of the strain gauges can be divided into many steps. Initially input channel is set by specifying the scan range. Then trigger by writing to the A/D low byte register (BASE +0) with any value wait for the end of conversion by reading the A/D status register (BASE +8). Now data from A/D converter is read by reading the A/D data registers. The binary digital data is converted to integer value, which is shown on the screen.

## 5.3 The Controller Board

A controller board is designed for real time control of all six motors through the printer port of the PC-AT 386. One board is designed to control four motors, so two such boards are used to control simultaneously all the six motors.

The basic scheme for control involves the principle of pulse width modulation. An asymmetric square wave is generated through the software. The duty cycle of the pulse wave form determines the relationship between the input and output voltage. Duty cycle is the ratio of ON time to the period of the pulse wave form. The motor is switched ON for a time  $t_{ON}$  and then switched OFF for a time  $t_{OFF}$ . This cycle is repeated. Thus the motor speed and torque can be varied by varying ON and/or OFF time intervals. Thus effectively the pulse width is used to change the motor torque as shown in Fig.(5.3).

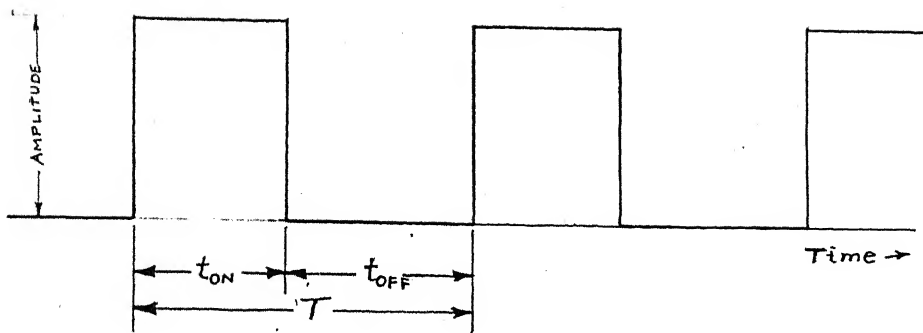


**Figure 5.3 : Pulse width Modulation with Square Wave form.**

In the meantime when one motor is kept OFF, other five motors are one by one switched ON and OFF to provide torque at all finger joints. The frequency of pulse is very high and when the motor is kept OFF, the object does not fall. The combined wave form for all six motors is shown in Fig.(5.4).

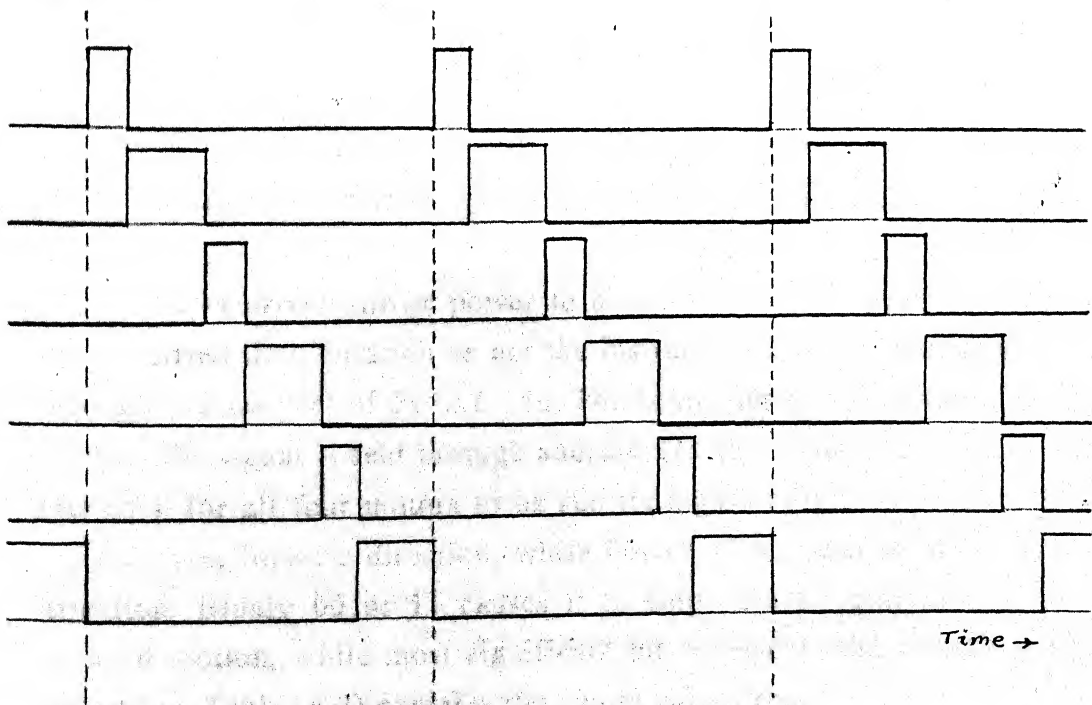


**Figure 5.4 : Schematic for Combined Pulse width Modulation.**

The controller board exchanges data from the printer port of PC-AT 386 and supplies power to all six motors in small pulses. 26-pin FRC from the printer is connected to controller board, where the signals go to L-298 dual full-bridge driver chip, whose block diagram is shown in Fig.(5.5).

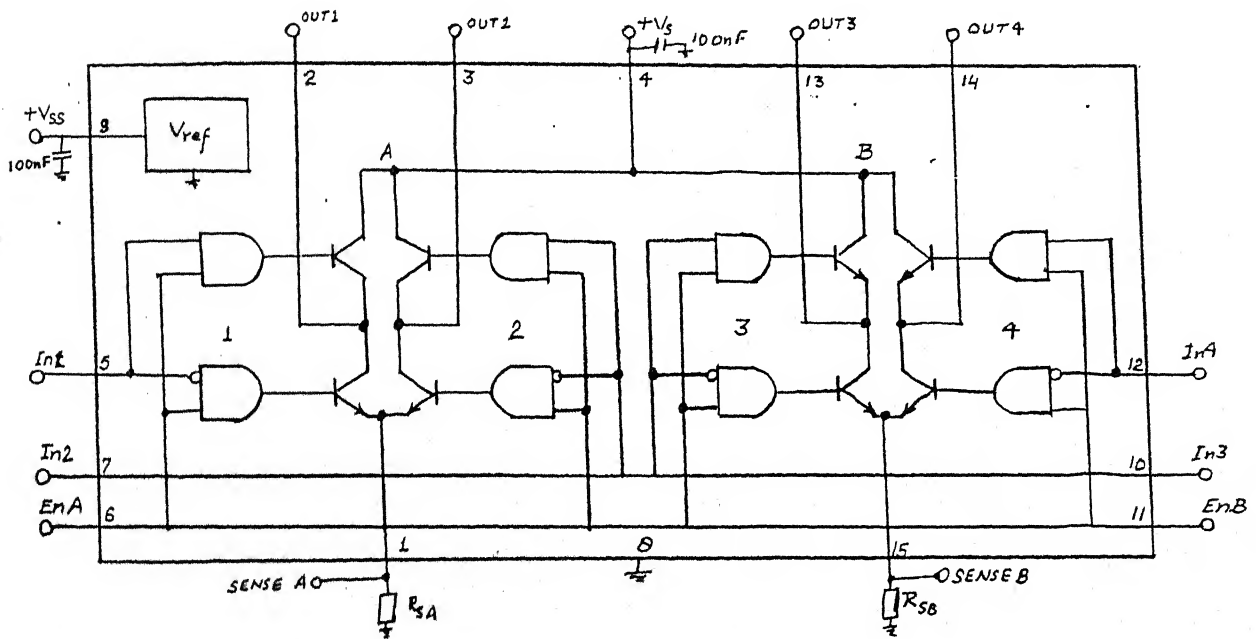


**Figure 5.5 : Block diagram for L-298 Dual Full Bridge driver.**

L-298 driver allows power to be supplied to the specified motor for the specified time duration as per the instructions from the software coming through printer port of PC-AT 386. For controller board-1 which controls 4 motors, the signal is sent through address 278 Hex. The 8-bit signal allows 2 bits each for all four motors to be run through board-1. A binary 01 moves the motor in forward direction, while binary 10 cause it to move in reverse direction. Binary 00 or 11 causes it to stop. Least significant bit denotes forward motion, while most significant bit represents the reverse motion of the motor. Table (5.2) contains the signal values required for various motion combinations.

Bit Allocation								Output	Hex	Motor	Motor	Motor	Motor
B2	B1	A2	A1					Signal	from	Motion	Motion	Motion	Motion
0	0	0	0	0	0	0	0	208	0x00	S	S	S	S
0	0	0	0	0	0	0	1	208	0x01	F	S	S	S
0	0	0	0	0	0	1	0	208	0x02	R	S	S	S
0	0	0	0	0	1	0	0	208	0x04	S	F	S	S
0	0	0	0	1	0	0	0	208	0x08	S	R	S	S
0	0	0	1	0	0	0	0	208	0x10	S	S	F	S
0	0	1	0	0	0	0	0	208	0x20	S	S	R	S
0	1	0	0	0	0	0	0	208	0x40	S	S	S	F
1	0	0	0	0	0	0	0	208	0x80	S	S	S	R

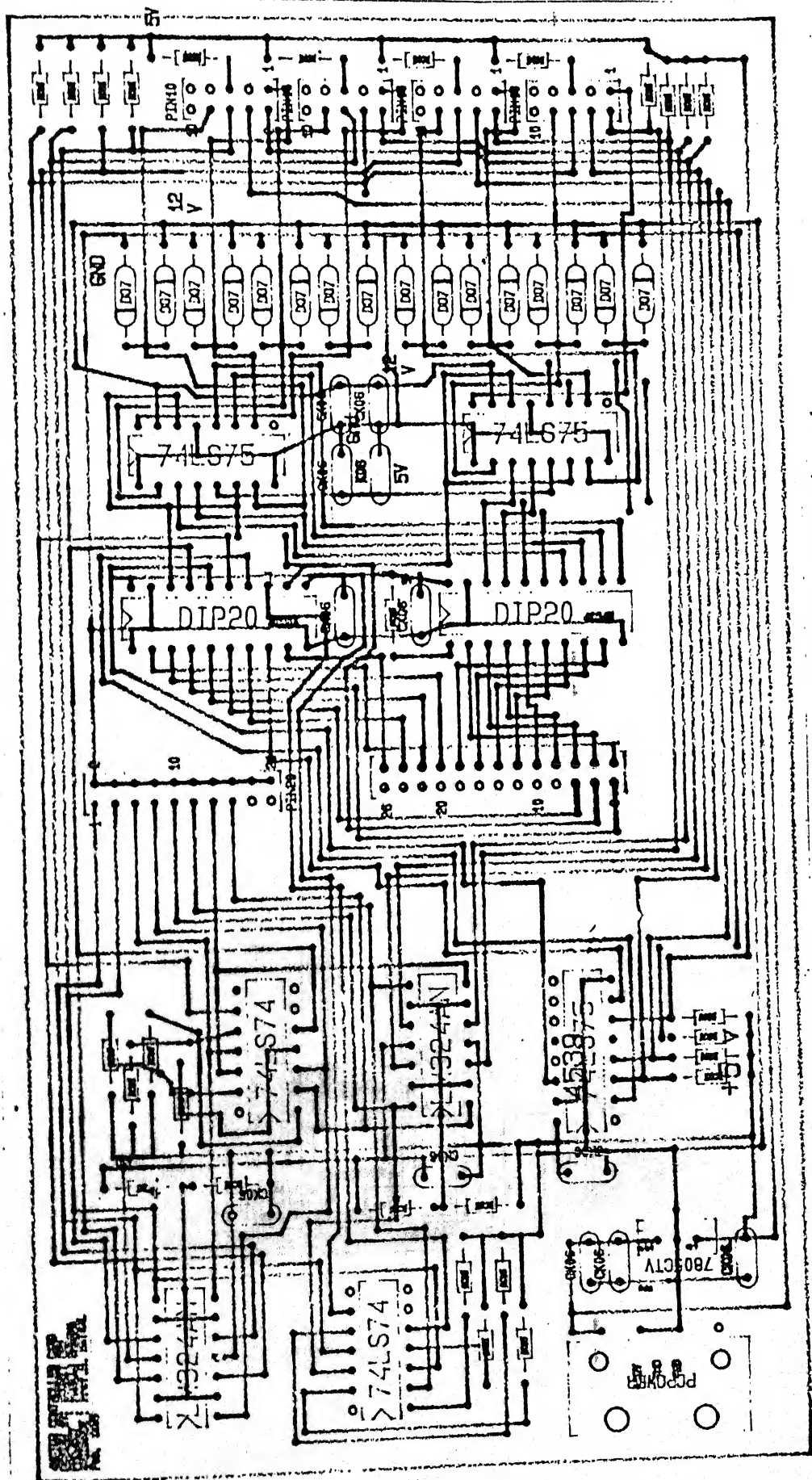
**Table 5.2 : Signals for Different Motor Motions.**

Using the logic in bit allocation for motors, various other combinations for simultaneous motions of two or more motors could be possible.

Similarly for controller board-2, which controls motors C1 and C2, the signal address is 27a Hex. Same logic is applied in bit allocation for motors C1 and C2 as presented above for board-1 except that the address changes to 27a Hex, instead of 278 Hex.

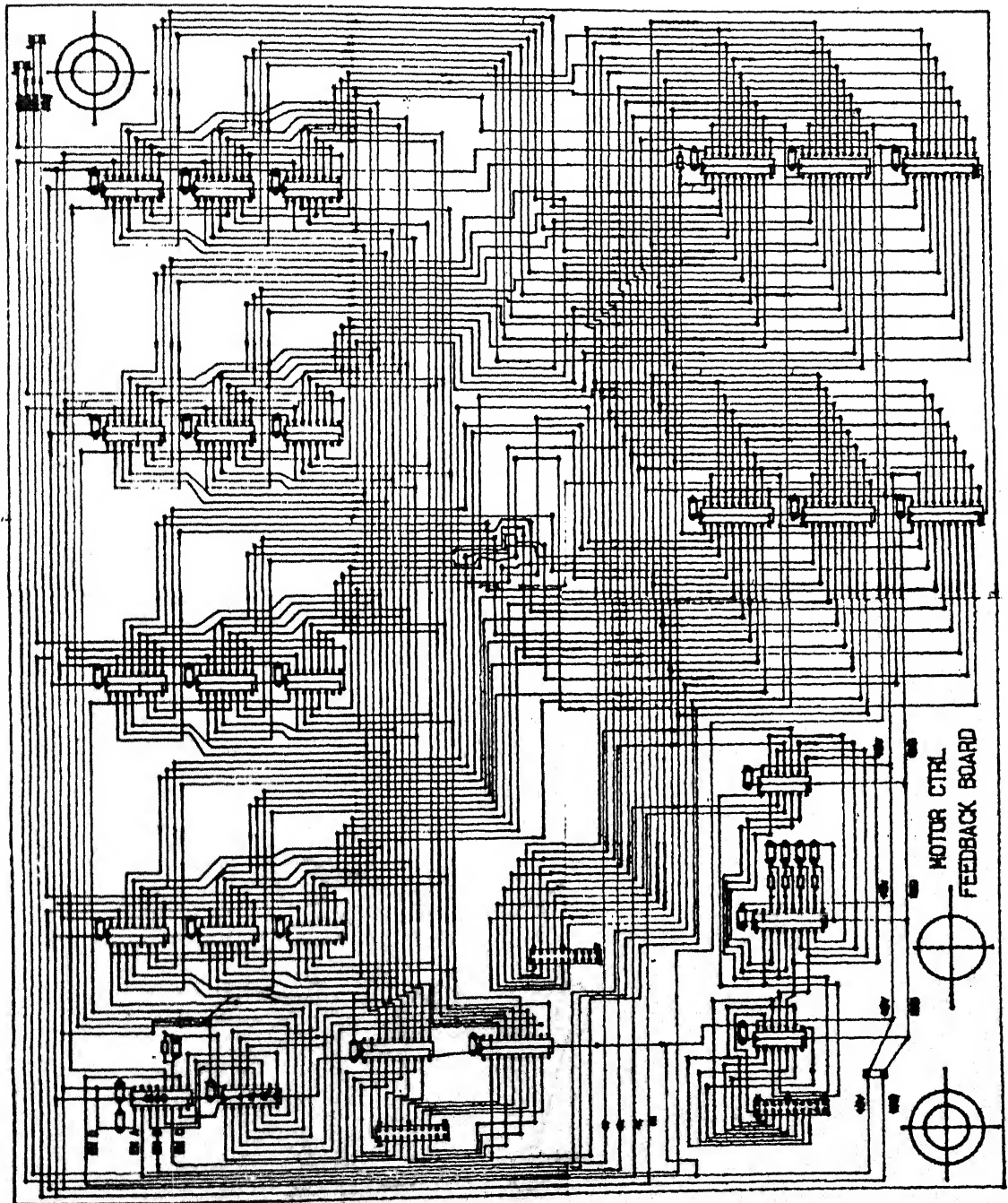
The PCB diagram for controller board is shown in Fig.(5.6).





## 5.6 PCB diagram for the controller board





5.7 PCB diagram for the feedback board

## 5.4 Feedback Board

The feedback board was planned to take the position feedback from the encoders and send it to PCL-812 enhanced multifunction card with AD-DA/DIO/TC facility. As motor shaft moves, the encoder keeps track of the rotation with respect to some reference point. This position status from the incremental encoder goes to feedback board, where information regarding direction of motion of the motor shaft is extracted from it. The encoder pulse increment or decrement is recorded and counted. The desired position of the motor is read from the PCL-812 card and the actual position of the status is sent to PCL-812 card. Unless the required position is reached the motor is moved in suitable direction. The PCB diagram for feedback board is shown in Fig.(5.7). This board could not be fabricated due to unavoidable circumstances.

Fig.(5.8) shows the nomenclature convention followed for naming the motors mounted on different fingers.

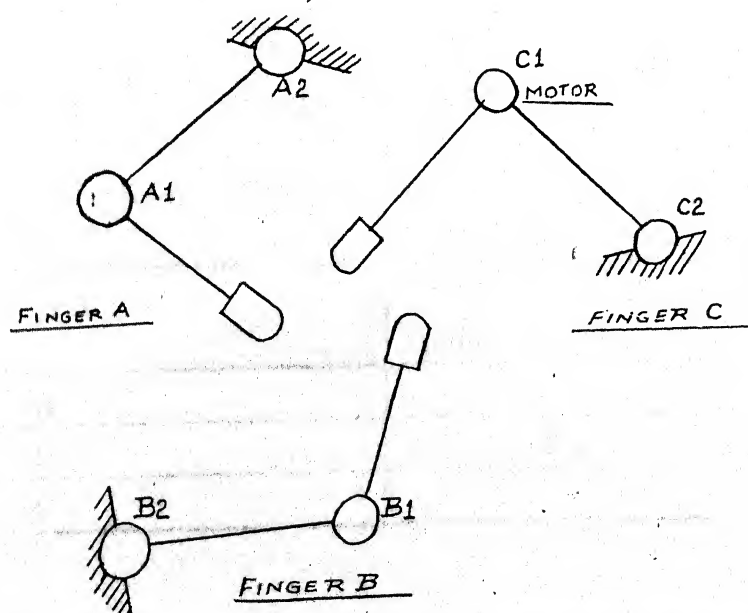


**Fig 5.8 : Nomenclature convention for Motors and Fingers.**

## 5.5 Results and Discussions

In the absence of feedback board, the position feedback could not be used and the closed-loop control scheme could not be applied. Therefore the objective was simplified to a stationary grasp of the object so that the fingers provide enough force to hold the object under gravity loading. This objective was achieved by open loop control of motor current. The current to motor was gradually increased till the object could be held without any slip. With the object held stationary, an attempt was made to correlate the motor current with the strain gauge reading.

The motors are controlled using the controller boards according to the principal of pulse modulation. The current passing through the motors is measured by measuring the voltage across a known resistance put in series with the motor. The current is varied by varying the proportion of positive pulse in one time period. Using the motor torque-constant data, the torque applied at each motor could be determined. This torque is converted to the force applied at the fingertips. This force is matched with the strain gauge feedback using the calibration chart. The nomenclature convention for motors followed is shown in Fig (5.8).

The observations for the strain gauges circuit output voltages for three fingers at the time of grasp are shown in Table(5.3). These observations are taken for transverse force on the fingertip.

Finger	Reading Shown on PC Terminal Screen (volts)
A	-2.5
B	-2.3
C	-1.4

**Table 5.3 : Output Voltage Observations.**

Using calibration chart as shown in the Fig.(5.1), we convert the Wheatstone bridge output voltage to force applied at the fingertip. The converted values for the transverse force ( $F_c$ ), are shown in the Table (5.4).

Finger	Bridge output voltage (value from the screen) (volts)	Transverse Force at the fingertip (N)
A	-2.5	0.2888
B	-2.3	0.2657
C	-1.4	0.1617

**Table 5.4 : Conversion Chart.**

The total cycle time and positive cycle time for each motor are recorded using portable digital oscilloscope. The rms voltage values across a known resistor of 5.3 ohm resistance value are also recorded for each motor. The observations are shown in the Table (5.5).

Motor	rms Voltage (Volts)	Positive Pulse width ( $\mu s$ )	Total Period (ms)	Frequency (Hz)
A1	1.46	214	2.48	403
A2	2.20	464	2.48	403
B1	1.18	174	2.48	403
B2	2.28	450	2.48	403
C1	1.14	150	2.48	403
C2	2.12	390	2.48	403

**Table 5.5 : Peak Voltage Observation.**

The rms current value with the 5.3 ohm resistance is calculated and shown in Table (5.6).

Motor	rms Voltage $V_{rms}$ volts	Resistance R ohms	rms Current $I_{rms} = V_{rms}/R$ Amps.	Torque $49.7 \times 10^{-3} I_{rms}$ Nm
A1	1.46	5.3	0.2755	0.0317
A2	2.28	5.3	0.4302	0.0214
B1	1.18	5.3	0.2226	0.0111
B2	2.28	5.3	0.4302	0.0214
C1	1.14	5.3	0.2151	0.0107
C2	2.12	5.3	0.4000	0.0199

**Table 5.6 : Current and Torque Calculations.**

Motor torque constant is 49.7mNm/A [Table 4.2], thus motor torque is calculated by multiplying motor torque constant with the rms current value.

The angles between the links are measured using the photographs taken for each link and the finger Jacobian matrix  $J_f$  is calculated as shown in equations(2.9) and (2.10).

The values for measured angles in degrees are shown in Table (5.7).

$\theta_1^1$	$\theta_2^1$	$\theta_1^2$	$\theta_2^2$	$\theta_1^3$	$\theta_2^3$
197	126	7	95	102	86

**Table 5.7 : Measured Joint Angles**

Here  $\theta_1^i, \theta_2^i$  ( $i=1,2,3$ ) are the joint angles for link-1 and link-2, respectively, for the  $i^{th}$  finger. Length for link-1 and link-2 is taken as 7.5 cm and 8 cm respectively.

The finger Jacobian matrix is calculated as

$$J_f = \begin{bmatrix} 0.07007 & 0.04815 & 0 & 0 & 0 & 0 \\ -0.00783 & 0.06389 & 0 & 0 & 0 & 0 \\ 0 & 0 & -0.08739 & -0.07825 & 0 & 0 \\ 0 & 0 & 0.05781 & -0.01663 & 0 & 0 \\ 0 & 0 & 0 & 0 & -0.06223 & 0.01113 \\ 0 & 0 & 0 & 0 & -0.09482 & -0.07922 \end{bmatrix} \quad (5.1)$$

The inverted Jacobian matrix is computed as

$$[J_f^T]^{-1} = \begin{bmatrix} 13.1616 & 1.6142 & 0 & 0 & 0 & 0 \\ -9.92239 & 14.4443 & 0 & 0 & 0 & 0 \\ 0 & 0 & -2.7827 & -9.6714 & 0 & 0 \\ 0 & 0 & 13.0918 & -14.6209 & 0 & 0 \\ 0 & 0 & 0 & 0 & -13.2358 & 15.8412 \\ 0 & 0 & 0 & 0 & -1.8692 & -10.3965 \end{bmatrix} \quad (5.2)$$

The position vector of contact points on object surface is as following

$$X = \begin{bmatrix} -0.069 \\ 0.011 \\ 0.034 \\ -0.023 \\ 0.053 \\ 0.046 \end{bmatrix} \quad (5.3)$$

From equation(2.35) we have  $\tau = J_f^T F_c$ . Thus we can write as

$$F_{c_{6 \times 1}} = [J_f^T]_{6 \times 6}^{-1} \tau_{6 \times 1} \quad (5.4)$$

The torque vector can be written from Table(5.6) as

$$\tau = \begin{bmatrix} 0.0137 \\ 0.0214 \\ 0.0111 \\ 0.0214 \\ 0.0107 \\ 0.0199 \end{bmatrix} \quad (5.5)$$

Calculating the contact force vector  $F_c$ , we have

$$F_c = \begin{bmatrix} 0.2149 \\ 0.1730 \\ -0.2379 \\ -0.1676 \\ 0.1736 \\ -0.2268 \end{bmatrix} \quad (5.6)$$

The Grip Transform matrix  $G$  is calculated [equations(2.31)-(2.32)] as

$$G = \begin{bmatrix} 1 & 0 & -0.011 \\ 0 & 1 & -0.069 \\ 1 & 0 & 0.023 \\ 0 & 1 & 0.034 \\ 1 & 0 & -0.046 \\ 0 & 1 & 0.053 \end{bmatrix} \quad (5.7)$$

From equations(2.37)-(2.38) the force  $F_o$  is calculated as

$$F_o = \begin{bmatrix} 0.1506 \\ -0.2214 \\ -0.0454 \end{bmatrix} \quad (5.8)$$

Thus the net resultant force on the object at the centre of object frame is 0.2677 N and net resultant torque about z-axis of the object frame is -0.0454Nm.

It is to be noted that the calculation(5.8) shows a net resultant force/torque on the object. However, in the actual experiment, the object was observed to be completely stationary for nearly 45 minutes. In order to resolve this discrepancy, some numerical trials were taken by varying the joint angle vector and the joint torque vector. It was observed that  $F_c$  is not very sensitive to small variations in the joint angle vector. Whereas  $F_o$ , and thus  $F_o$ , was found to change significantly with small changes in the joint

torque vector  $\tau$ . For example, with an assumed  $\tau$  vector as  $\begin{bmatrix} 0.0107 \\ 0.0227 \\ 0.0173 \\ 0.0210 \\ 0.0105 \\ 0.0129 \end{bmatrix}$  which is

close to the one in equation(5.5),  $F_c$  was calculated to be

$$F_c = \begin{bmatrix} 0.1775 \\ 0.2216 \\ -0.2512 \\ -0.0806 \\ 0.0654 \\ -0.1536 \end{bmatrix} \quad (5.9)$$

and  $F_o$  was computed as

$$F_o = \begin{bmatrix} -0.0084 \\ 0.0126 \\ -0.0368 \end{bmatrix}. \quad (5.10)$$

Here the net resultant force  $F_o$  reduces from 0.2677N [see(5.8)] to 0.0151N[see(5.10)].

In fact,  $\tau$  was calculated by reading the rms value of voltage across the resistance (as shown in Table(5.6)). The pulse width modulation to control the motor current is shown in Fig(5.4). Since there is no way to measure the actual current to the motor, the torque calculations were based on rms values. This procedure is obviously not accurate. The transverse component ( $F_c$ ), values as shown in Figs.(4.6) and (4.16) for the three-fingers are shown in Table(5.8).

Finger	Transverse force component from equation(5.6).	Transverse force component from strain gauge readings. [Table(5.3)-(5.4)]	Transverse force component [equation(5.9)] for the assumed torque vector close to the original one given in eqn.(5.5)
A	0.2675	0.2888	0.2838
B	0.2625	0.2657	0.2625
C	0.2488	0.1657	0.1612

**Table 5.8 : Transverse components for the three-fingers**

From Table(5.8) it is clear that the strain gauge readings for transverse force for the three-fingers match with the values in the last column of Table(5.8). The values in the last column of Table(5.8) give net resultant force on the origin of the object frame very near to zero which means that the grasp was stable for the static case. In actual experiment also, the object was



observed to be completely stationary. Thus the values of the transverse force for the three-fingers in columns three and four of Table(5.8) are in accordance with each other. The values in the second column does not match with the strain gauge output, since there is no way to measure the actual current to the motor.

In the full real time implementatation with closed-loop control, there is no need to measure the current. The current will be controlled directly through the feed back loop.

# Bibliography

---

[Andeen, 1988] Gerry B. Andeen(ed.), *Robot Design Handbook*, McGraw-Hill Book Company, 1988.

[Asada, 1986] H. Asada, J.J.E. Slotine, *Robot Analysis and Control*, John Wiley & Sons, 1986.

[Asada, 1987] Haruhiko Asada, Kamal Youcef-Toumi, *Direct Drive Robots: Theory and Practice*, The MIT Press, 1987.

[Bicchi, 1995] A. Bicchi, "On the Closure Properties of Robotic Grasping", in *International Journal of Robotics Research*, vol. 14, No. 4, pp. 319-334, 1995.

[Chung, 1993] W.Y. Chung, K.J. Waldron, "Force Distribution by Optimizing Friction Angles for Multifingered System", in *Proceedings of the 1993 IEEE Conference on Robotics & Automation*, pp. 717-722, 1993.

[Chung, 1995] W. Chung, K.J. Waldron, "An Integrated Control Strategy for Multifingered Systems", in *Transactions of ASME, Journal of Dynamics, Systems, Measurements and Control*, vol. 117, pp. 37-42, 1995.

[Cole, 1992] Arlene A. Cole, Ping Hsu, S. Shankar Shastri, "Dynamic Control of Sliding by Robotic Hands for Regrasping", in *IEEE Transactions on Robotics and Automation*, vol. 8, No. 1, pp. 42-52, Feb. 1992.

[Craig, 1986] John J. Craig, *Introduction to Robotics Mechanics and Control*, Addison-Wesley Publishing Company, 1986.

[Crossley, 1977] F. Crossley, F. Umholtz, "Design for a Three Fingered Hand", in *International Journal of Mechanism and Machine Theory*, vol. 12, pp. 37-49, 1977.

[Cutkosky, 1985] Mark R. Cutkosky, *Robotic Grasping and Fine Manipulation*, Kluwer Academic Publishers, 1985.

[Cutkosky, 1989] Mark R. Cutkosky, "On Grasp Choice, Grasp Models and the Design of Hands for Manufacturing Tasks" in *IEEE Transactions on Robotics and Automation*, vol. 5, No. 3, pp. 269-279, 1989.

[Duffy, 1996] Joseph Duffy, *Statics and Kinematics with Applications to Robotics*, Cambridge University Press, 1996.

[Fearing, 1986] R.S. Fearing, "Implementation of a Force Strategy for Object Reorientation", in *Proceedings of the 1986 IEEE Conference on Robotics and Automation*, pp.96-102, 1986.

[Fu, 1987] K.S. Fu, R.C.Gonzalez, C.S.G. Lee, *Robotics: Control, Sensing, Vision, and Intelligence*, McGraw-Hill Book Company, 1987.

[Guo, 1993] G.Guo, W.Gruver, "Optimal Distribution of Fingertip Force Functions in Dynamic Grasping " , in *Proceedings of the 1993 IEEE Conference on Robotics and Automation*, pp. 971-977, 1993.

[Hahm, 1988] Geon Hahm, "Semiconductor Strain Gages" in John G. Webster (ed.), *Tactile Sensors for Robotics and Medicine*, John Wiley & Sons, 1988.

[Kerr, 1986] J.Kerr, B.Roth, "Analysis of Multifingered Hands", in *International Journal of Robotics Research*, vol. 4, No. 4, pp. 3-17, 1986.

[Klafter, 1989] Richard O. Klafter, Thomas A. Chmielewski, Michael Negin, *Robotic Engineering: An Integrated Approach*, Prentice Hall of India, 1989.

[Kobayashi, 1986] H. Kobayashi, "Control and Geometric Considerations for an Articulated Robot Hand", in *International Journal of Robotics Research*, Vol. 4, no1, pp. 3-12, 1986.

[Kumar, 1988] V.R. Kumar, K.J. Waldron, "Force Distribution in Closed Kinematic Chains", in *IEEE Journal of Robotics and Automation*, vol. 4, No. 6, pp. 657-664, 1988.

[Kumar, 1989] V.R. Kumar, K.J. Waldron, "Sub-optimal Algorithms for Force Distribution in Multifingered Grippers", in *IEEE Transactions of Robotics and Automation*, vol. 5, No. 4, pp. 491-497, 1989.

[Kvrgic, 1996] Vladimir M. Kvrgic, "Computing of the Sub-optimal Grasping Forces for Manipulation of a Rough Object by Multifingered Robot Hand", in *Proceedings of the 1996 IEEE International Conference on Robotics and Automation*, pp. 1801-1806, April 1996.

[Li, 1989] Z. Li, P. Hsu, S. Sastry, "Grasping and Coordinated Manipulation by a Multifingered Robot Hand", in *International Journal of Robotics Research*, vol. 8, No. 4, pp. 33-50, 1989.

[Mackawa, 1996] Hitoshi Mackawa, Kazuo Tanie, Kiyoshi Komoriya, "Dynamic Grasping Force Control Using Tactile Feedback for Grasp of

Multifingered Hand", in *Proceedings of the 1996 IEEE International Conference on Robotics and Automation*, pp. 2462-69, April 1996.

[Mason, 1986] Matthew T. Mason, J. Kenneth Salisbury, Jr., *Robot Hands and the Mechanics of Manipulation*, The MIT Press, 1986.

[McDonald, 1986] Anthony C. McDonald, *Robot Technology: Theory, Design and Applications*, Prentice Hall, 1986.

[Montana, 1995] D. Montana, "The Kinematics of Multifingered Manipulation", in *IEEE Transactions on Robotics and Automation*, vol. 11, No. 4, pp. 491-503, 1995.

[Mukerjee, 1992] S. Mukerjee, K. Waldron, "Exact Optimization of Interaction Forces in Three Fingered manipulation", in *Transactions of ASME, Journal of Mechanical Design*, vol. 114, No. 1, pp. 48-55, 1992.

[Nagrath, 1985] I.J. Nagrath, M. Gopal, *Control Systems Engineering*, Wiley Eastern Ltd., (sixth reprint) 1985.

[Nahon, 1992] M. Nahon, J. Angeles, "Real Time Force Optimization in Parallel Kinematic Chains under Inequality Constraints", in *IEEE Transactions on Robotics and Automation*, vol. 8, No. 4, pp. 439-450, 1992.

[Nguyen, 1986] V. Nguyen, "The Synthesis of Stable Grasps in the Plane", in *Proceedings of the 1986 IEEE Conference on Robotics and Automation*, pp. 884-889, 1986.

[Nof, 1985] Shimon Y. Nof (ed.), *Handbook of Industrial Robotics*, John Wiley & Sons, 1985.

[Ogata, 1986] Katsuhiko Ogata, *Modern Control Engineering*, Prentice Hall of India Pvt. Ltd., 1986.

[Okada, 1979] T. Okada, "Object Handling System for Manual Industry", in *IEEE Transactions on Systems, Man and Cybernetics*, vol. 9, No. 2, pp. 79-89, 1979.

[Omata, 1994] T. Omata, K. Nagata, "Planning Reorientation of a Object with a Multifingered Hand", in *Proceedings of the 1994 IEEE Conference on Robotics and Automation*, pp. 3104-3110, 1994.

[Rao, 1971] C. Rao , S.Mitra, *Generalised Inverse of Matrices and its Applications*, John Wiley & Sons, 1971.

[Rivin, 1988] Eugene I. Rivin, *Mechanical Design of Robots*, McGraw-Hill Book Company, 1988.

[Salisbury, 1989] Kenneth Salisbury, David Brook, and Patrick O'Donnel, "Using an Articulated Hand to Manipulate Objects" in Michael Brady (ed.), *Robotics Science*, The MIT Press, 1989.

[Schilling, 1990] Robert J. Schilling, *Fundamentals of Robotics Analysis and Control*, Prentice Hall, 1990.

[Shimoga, 1996] K. Shimoga, "Robot Grasps Synthesis Algorithms : A Survey", in *International Journal of Robotics Research*, vol. 15, No. 3, pp. 230-266, 1996.

[Spong, 1989] M.W. Spong, M. Vidyasagar, *Robots Dynamics and Control*, John Wiley & Sons , 1989.

[Stone, 1987] Henry W. Stone, *Kinematic Modeling, Identification and Control of Robotic Manipulators*, Kluwer Academic Publishers, 1987.

[Yoshikawa, 1990] Tsuneo Yoshikawa, *Foundations of Robotics: Analysis and Control*, The MIT Press, 1990.

[Yoshikawa, 1991] T. Yoshikawa, K. Nagai, "Manipulating and Grasping Forces in Manipulation by Multifingered Robot Hands", in *IEEE Transactions on Robotics and Automation*, vol. 7, No. 1, pp. 67-77, Feb. 1991.

**141996**  
**Date Slip**

[illegible]

A141996